atmosphere

MDPI

Article

Seasonality of Precipitation over Himalayan Watersheds in CORDEX South Asia and their Driving CMIP5 Experiments

Shabeh ul Hasson [1,2]

[1] CEN, Institute of Geography, University of Hamburg, Hamburg 20146, Germany; shabeh.hasson@uni-hamburg.de

[2] Department of Space Sciences, Institute of Space Technology, Islamabad 44000, Pakistan

Academic Editor: Katja Friedrich

Received: 26 July 2016; Accepted: 22 September 2016; Published: 2 October 2016

Abstract: Since the Coupled Model Intercomparison Project Phase 5 (CMIP5) experiments exhibit limited skill in reproducing the statistical properties of prevailing precipitation regimes over the major Himalayan watersheds (Indus, Ganges, Brahmaputra and Mekong), this study evaluates the anticipated added skill of their dynamically refined simulations performed under the framework of Coordinated Regional Climate Downscaling Experiments for South Asia (CX-SA). For this, the fidelity of eight CX-SA experiments against their six driving CMIP5 experiments is assessed for the historical period (1971–2005) in terms of time-dependent statistical properties (onset/retreat timings and rapid fractional accumulation—RFA) of the dominant summer monsoonal precipitation regime (MPR). Further, a self-defining seasonality index (SI), which is a product of precipitation and the distance of its actual distribution relative to its uniform distribution (relative entropy—RE), has been computed for MPR, westerly precipitation regime (WPR) and annual precipitation. The time evolution of precipitation, RE and SI has also been analyzed. Results suggest that CX-SA experiments simulate even higher wet biases than their driving CMIP5 experiments over all study basins, mainly due to higher wet biases simulated over the Himalayas and Tibetan Plateau. Most of the CX-SA experiments suggest unrealistic timings of the monsoon onset that are far earlier than their driving CMIP5 experiments for all basins. Generally, CX-SA experiments feature higher underestimation of RFA slope, RE and SI, distancing their driving CMIP5 experiments farther from observations. Interestingly, regardless of the diverse skill of CMIP5 experiments, their fine scale CX-SA experiments exhibit quite a similar skill when downscaled by the same regional climate model (RCM), indicating RCM's ability to considerably alter the driving datasets. These findings emphasize on improving the fidelity of simulated precipitation regimes over the Himalayan watersheds by exploiting the potential of RCMs in term of microphysics, resolutions and convective closures, and preferably, on resolving the crucial fine scale processes further down to their representative (meso-to-local) scales.

Keywords: precipitation; seasonality; Himalayan watersheds; CORDEX South Asia; CMIP5

1. Introduction

The sustainable development of agrarian economies and the well-being of a billion people are at stake, if the future of the water availability from the Himalayan watersheds remains uncertain. It is particularly a serious concern in the wake of climate change, its recent acceleration and now established elevation dependent warming, suggesting amplified warming over the elevated regions, such as, the Himalayas [1–4]. The assessment of future water availability for the Himalayan watersheds requires, above all, a valid set of climate change projections, for which

the present-day state-of-the-art climate modeling tools are a primary source [5]. An extensive development of these climate modeling tools have raised the expectations of their robust support in assessing the climate change impacts on various sectors of life, in devising the subsequent national action plans, and in the policy development. However, the reliability of projected hydroclimatic changes from these climate models largely depends upon the degree of their skill in two aspects: in adequately representing the physical hydroclimatic processes, and in reproducing well the observed hydroclimatic phenomenon, collectively called 'fidelity'. The robust fidelity assessment in turn requires a valid observational database.

The South and Southeast Asia features a complex hydroclimatolgy, which is largely determined by the prevailing weather systems—the summer monsoon and the subtropical cyclones—and their associated precipitation regimes, namely, the monsoonal precipitation regime (MPR) and the westerly precipitation regime (WPR) [4,6–9]. Hence, the reliability of climate model's projections for future changes in the hydrology of the region largely depends upon their realistic representation of both MPR and WPR for the present-day climate. While many studies that assess the representation of precipitation regimes in the climate models have focused on the reproducibility of the magnitude of precipitation, its geographical distribution, its temporal evolution or its extremes [7,10–14], less attention has been given to the representation of the seasonal cycle and to the overall seasonality [15–17]. Changes in the seasonality of precipitation regimes directly affect the timings of the water availability and are related to the risks of droughts and floods [18].

Few studies focusing only on the dominant MPR assess how well its statistical properties, such as the duration and the onset/retreat timings, are reproduced by the models; for the latter typically an absolute threshold of 5 mm·day^{-1} has been applied [10,19]. However, in view of a large spread of the simulated precipitation amid the climate models—owing to their structural limitations of adopted experimental setups and chosen physics—applying the absolute thresholds for determining the monsoon onset/retreat timings seems inadquate [20,21]. Similar is true when accounting for the spatial heterogeneity of MPR across its domain, as some (dry) models fail to achieve the absolute thresholds over the regions lying at the monsoon margins where the total incident precipitation is too little (e.g., Indus basin) [20,22]. Further, a dry (wet) bias may suggest a delayed (early) onset timing, yielding a biased length of the active monsoon duration (onset-retreat) and distinct extents of the monsoonal domain [10,20,23]. Given such limitations, the fidelity of the climate model experiments in representing the statistical properties of MPR should be assessed on a qualitative scale. This can be achieved either by applying the relative thresholds on the smoothed datasets or employing the self-defining threshold-independent measures.

A few relevant studies that focus on the qualitative fidelity assessment report contradictory findings. For instance, an application of the relative threshold of 0.2 on the All-India (65° to 85°E and 7° to 25°N) averaged fractional accumulated pentad precipitation from the coupled model intercomparison project (CMIP) phase 5 experiments suggests a delayed onset and a systematic bias in the phase of the annual cycle of MPR [23]. On a sub-regional scale, however, applying uniformly a relative threshold of 0.17 on the normalized monthly basin-integrated precipitation from the CMIP3 experiments indicates a varying skill of such experiments in suggesting the realistic monsoon onset timings across the Himalayan watersheds. Lately, applying the distinct relative thresholds for each Himalayan watershed on the basin-integrated pentad precipitation from the CMIP5 experiments, the study reports a modest skill of these experiments in suggesting the realistic onset timings for Ganges [20], which is in contrast to the earlier findings [23]. Similarly, for the precipitation concentration within the active monsoon duration, the skill of the CMIP5 experiments was found different when the active monsoon duration was identified by applying a uniform threshold over the whole study region [23], compared to when the distinct thresholds were used for each respective Himalayan watershed [20]. Such contradictory findings emphasize on the assessment of the statistical properties of MPR on a sub-regional scale, such as the Himalayan watersheds, as well as on applying the distinct relative thresholds for each watershed.

Nevertheless, the above mentioned studies have demonstrated a limited skill of the CMIP3 and CMIP5 experiments in the realistic representation of MPR. This is largely due to the structural limitations of the participating coupled climate models, and in turn, to their oversimplified representation of the region-specific geophysical features and the associated hydroclimatic processes and feedback. Since the regional climate models (RCMs) somewhat overcome such structural limitations due to their finer resolution, they are typically believed to outperform the coarse resolution CMIP3/CMIP5 experiments. Lately, a suite of fine-scaled (0.44°) derivatives of several CMIP5 experiments was made available for the South Asian domain (19.88° to 115.55°E and −15.23° to 45.07°N) under a common framework of the coordinated regional climate downscaling experiments (CORDEX) [24,25], onward referred to as CX-SA. Against this background, it is pertinent to analyze how well CX-SA experiments represent WPR and MPR relative to their driving CMIP5 experiments.

Hence, extending the previous analysis on the assessment of CMIP5 experiments in representing the prevailing precipitation regimes over major Himalayan watersheds of Indus, Ganges, Brahmaputra and Mekong, this study assesses the fidelity of eight fine-scaled CX-SA experiments relative to their six driving CMIP5 experiments. The skill metrics considered for the dominant MPR include the onset/retreat timings and the precipitation concentration within the active monsoon duration, which have been analyzed by applying the distinct relative-thresholds on the basin-integrated pentad precipitation for the historical period (1971–2005). Since such skill metrics confines to the active monsoon duration only and cannot be equally applied to WPR, the seasonality of the overall precipitation regimes has been additionally assessed. For this, a self-defining quantitative measure of the overall seasonality of precipitation regime, called seasonality index (SI), has been applied separately to MPR, WPR and annual precipitation. The SI is a product of precipitation and the Kullback-Leibler divergence [26] or relative entropy (RE)—an information-theory based measure of divergence of actual precipitation distribution from its uniform distribution [15,16,27]. In order to see the time evolution of changes in the seasonality of prevailing precipitation regimes over the historical period, trends in SI along with trends in precipitation and RE have been analyzed using the Mann-Kendall trend test.

2. Study Area

The study region comprises of four major river basins of south and southeast Asia, namely, Indus, Ganges, Brahmaputra and Mekong (Figure 1). The hydrology of these basins is nourished by spatially incoherent, seasonally bifurcated and heterogeneous form of precipitation (snow or rain) input under two distinct precipitation regimes; WPR is associated with the extra-tropical westerly disturbances that originate from the Caspian or the Mediterranean Seas while MPR is associated with the southwest summer monsoon system that comes from the Bay of Bengal and the Arabian Sea [8,22,28]. Being transported to their far-eastern extremity over the study basins through the southern flank of the Atlantic and Mediterranean storm tracks [29], the year-round westerly disturbances drop moisture mainly during winter and spring, mostly in the solid form and largely over the Karakoram region within the upper Indus basin. The influence of these disturbances is somewhat evident over the Brahmaputra headwaters too, but negligible over Ganges and Mekong. On the other hand, the late-spring surface-level differential solar heating amid the land and the ocean as well as the Tibetan Plateau's sensible heating of the mid-to-upper troposphere result into a meridional pressure gradient responsible for generating a cross-equatorial monsoonal surface flow [30,31]. Such monsoonal surface flow is bifurcated into several branches that pick moisture from different parts of the ocean and drop it over different parts of the land. An abrupt but consistent precipitation increase overland is generally referred to as the monsoon onset, which first hits the southern India and the lower Mekong in late-May, and then advancing north and northwestward, reaches over the Brahmaputra shortly, over the Ganges in June, and over the Indus in July [32,33]. The withdrawal of the monsoon refers back to the pre-onset dry conditions that gradually retreat roughly in the onset order, latest by October/November [32,33].

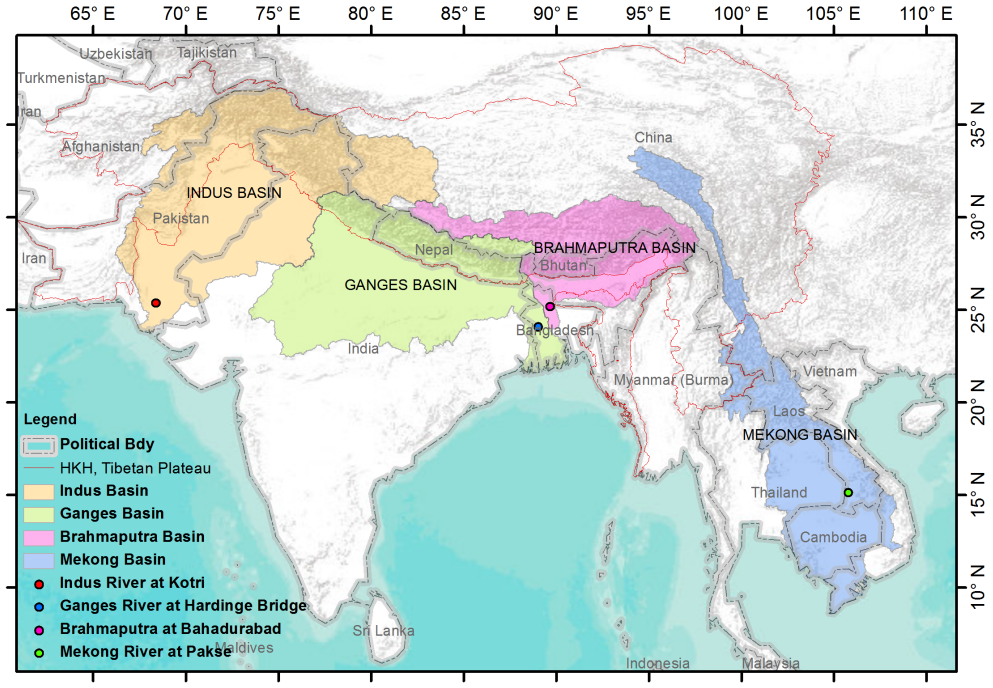

Figure 1. Major South and Southeast Asian river basins.

The eastern basins are under the dominant influence of MPR and receive mostly the rainfall over their lower plains during the summer monsoon period. In contrast, the hydrology of Indus is governed by the both WPR and MPR; the snow is received under WPR mainly during winter and spring while the rain (snow) is received under MPR at low (high) altitudes during summer. Hence, Indus features a more complex hydroclimatology than other three basins. The eastern basins are wetter in terms of the both precipitation and discharge than the western basins where the agriculture is a major consumer of the available water. The agriculture within the eastern basins is mostly rain-fed, and thus, is sensitive to the timings of the monsoon onset. Featuring extensive irrigation and shorter monsoon duration, the western basins are additionally sensitive to the magnitude of precipitation and to the length of the active monsoon duration, whereas Indus additionally depends heavily on the melting of snow received under WPR [34].

3. Data Used

As for the observational datasets (OBS), precipitation was obtained from: (1) the Asian Precipitation-Highly Resolved Observational Data Integration Towards Evaluation (APHRODITE—onward APHRO) of Water Resources version VR1101 [35]; (2) the Global Precipitation Climatology Project (GPCP) [36], and; (3) the CPC Merged Analysis of Precipitation (CMAP) [37]. The APHRO is a station interpolated gridded dataset available at the daily temporal and 0.5° planar resolution for the period 1951–2007. The GPCP and CMAP datasets are multi-source satellite-merged gridded observations available at the pentad temporal and 2.5° planar resolution since 1979. The GPCP has been obtained from integrating the microwave- and infrared-derived estimates with the in-situ gauge observations while CMAP additionally integrates estimates from the outgoing long-wave radiation and—in place of in-situ observations—NCEP-NCAR reanalysis [37–39]. The considered datasets have been widely used for studying the hydrological cycle on global and regional scales.

In view of the observational uncertainty—caused by location and elevation biased in-situ observations, by their regionalization schemes in the complex HKH terrain and by the limited skill of the remote sensing platforms in estimating precipitation [4,20,34,35,40–42]—the multiple observational datasets have been used in the analysis.

For the climate model simulations, the daily precipitation for the period of 1971–2005 was taken from the eight fine scaled (0.44° resolution) CX-SA experiments, which are obtained by dynamically downscaling six CMIP5 experiments [43] using three different RCMs (Table 1). In order to analyze the added value of the fine scaled CX-SA experiments, the daily precipitation from their six driving CMIP5 experiments was also obtained.

Table 1. The CX-SA and their driving CMIP5 experiments, employed RCM and contributing institutes.

S No	Experiment Name	RCM Employed/Experiment Contributing Institute	Driving GCM	GCM Resolution (lat° × lon°)
1	ACCESS1-0_CCAM	CCAM [44]—Conformal-Cubic Atmospheric Model/ Commonwealth Scientific and Industrial Research Organization (CSIRO), Marine and Atmospheric Research, Australia	ACCESS1-0 [45]	∼1.25° × 1.875°
2	CCSM4_CCAM	CCAM / CSIRO	CCSM4 [46]	∼0.942° × 1.25°
3	CNRM-CM5_CCAM	CCAM/CSIRO	CNRM-CM5 [47]	∼1.400° × 1.406°
4	EC-EARTH_RCA4	RCA4 [48]—Rossby Centre regional atmospheric model version 4-2/Swedish Meteorological and Hydrological Institute, Sweden	EC-EARTH [49]	∼1.121° × 1.125°
5	GFDL-CM3_CCAM	CCAM/CSIRO	GFDL-CM3 [50]	∼2° × 2.5°
6	MPI-ESM-LR_CCAM	CCAM/CSIRO	MPI-ESM-LR [51]	∼1.865° × 1.875°
7	MPI-ESM-LR_REMOi	REMO [52,53]—Regional Model for climate simulations/Helmholtz-Zentrum Geesthacht, Climate Service Center and Max Plank Institute for Meteorology, Germany		
8	MPI-ESM-LR_REMO			

4. Methods

The daily precipitation from APHRO, CX-SA and CMIP5 was converted into pentad precipitation while the coarse resolution datasets of GPCP, CMAP and CMIP5 were bilinearly interpolated to a common resolution of CX-SA experiments (0.44°). For the climate model fidelity assessment over the south Asia, earlier studies have either focused on a model grid cell or on a whole study region. However, it is strongly believed that the evaluation on a local grid cell is too stringent for the coarse resolution climate models due to the possibility of small spatial offsets in their simulated fields. Whereas, in view of the tremendous spatial heterogeneity of the hydroclimatic characteristics of the study region, a regional scale model performance may vary from that of assessed on a sub-regional scale. Thus, the model evaluation should additionally be performed on a sub-regional scale, such as, the river basin, which is quite a relevant unit for the practical water resource management. Hence prior to the analysis, the precipitation for each pentad from all gridded datasets was integrated over the Himalayan watersheds using Equation (1), in order to precisely measure precipitation within the natural watershed boundaries.

$$(p)_{i,k} = \frac{1}{A}\int_A q_{i,k}\,dA \tag{1}$$

where A is the basin area, $q_{i,k}$ represents precipitation quantity at a particular grid cell for the pentad, i, and the year, k, while $(p)_{i,k}$ is the basin-integrated pentad precipitation of the same pentad.

The integration procedure first converts the climate model grid into a tessellated surface using the Thiessen polygon method [54] in order to compute the representative area of each grid cell, and then weighs the incident precipitation at each grid cell according to its extent lying within the natural boundary of the basin. The weighted precipitation is then integrated over the basin divided by its surface area. This procedure is insensitive to the structure of the model grid and its resolution as described in detail in [5,22].

Skill Metrics

Since the water availability within the study basins is quite sensitive to the statistical properties of the dominating MPR, the climate models fidelity in terms of reproducibility of these properties has been assessed. In order to circumvent the effect of a large multi-model scatter, the quantities are first accumulated through the annual course and then their fractional accumulations are computed using Equations (2) and (3), respectively. The Figure 2a–c demonstrates how the inter-model spread of the simulated precipitation has been avoided.

$$\prod_t = \sum_{i=1}^{t} (p)_i \tag{2}$$

$$\tilde{\prod_t} = \prod_t / \prod_{73} \tag{3}$$

where t indicates each pentad within a year, $\prod_t$ is the accumulated (p) while $\tilde{\prod}_t$ is the fractional accumulated (p) at pentad, t.

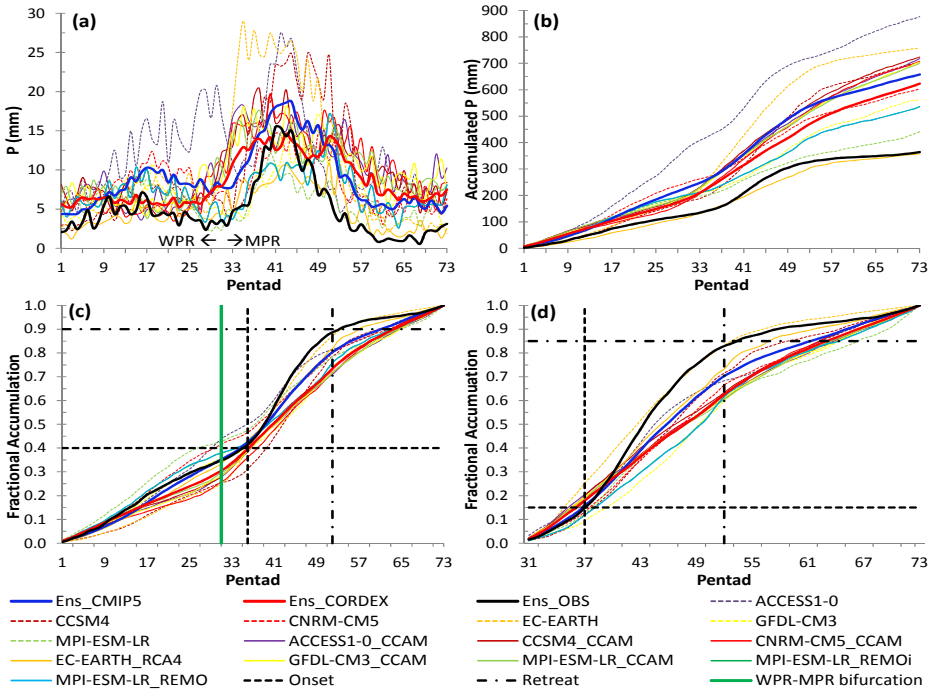

Figure 2. The inter-model spread of the basin-integrated pentad precipitation for Indus basin from CORDEX South Asia and their driving CMIP5 experiments and ensemble means in: (**a**) climatological annual cycle (mm); (**b**) accumulated precipitation (mm); (**c**) fractional accumulated precipitation; (**d**) fractional accumulation excluding January to May period of WPR.

The climatological annual cycle of $\prod$ and $\tilde{\prod}$ from the considered observations are plotted in Figure 3. Based on the climatological $\tilde{\prod}$ of GPCP, the relative thresholds that yield right timings of the basin-wide monsoon onset/retreat were distinctly identified for each basin. The relative threshold for the observed monsoon onset (retreat) timing was defined as the fractional accumulation at the pentad, t, which satisfies two conditions: (1) a rapid linear growth in $\tilde{\prod}$ starts right after the pentad, t; (2) the timing of the pentad, t, tallies with the timing of the basin-centered observed climatological onset (retreat) isochrone, as reported by [32] from GPCP over the period 1979–1999 and by the Indian Meteorological Department (IMD) from the long-term station record [33]. For instance, the rapid fractional accumulation for Ganges starts right after the pentad 32 whose timing of 9 June coincides

well with the observed climatological onset isochrone around the middle of Ganges (Figure 3). Thus, $\tilde{\prod}_{32}$ has been taken as the relative threshold for identifying the observed onset timing. Using similar approach, the relative thresholds that identify the right timings of the monsoonal retreat have been identified for each basin. As mentioned afore in Section 2, Indus comes under the influence of both WPR and MPR, featuring a bimodal precipitation distribution (Figure 2). In order to circumvent the influence of WPR on identifying the timings of MPR onset, $\prod$ and $\tilde{\prod}$ for Indus were computed for $t = 31...73$, excluding the January–May period. The additional skill metrics considered was the growth rate of $\tilde{\prod}$ from the onset to the retreat pentads that represents a measure of concentration of precipitation within the active monsoon duration. Such growth rate has been computed as a linear regression slope, onward called as the rapid fractional accumulation (RFA) slope.

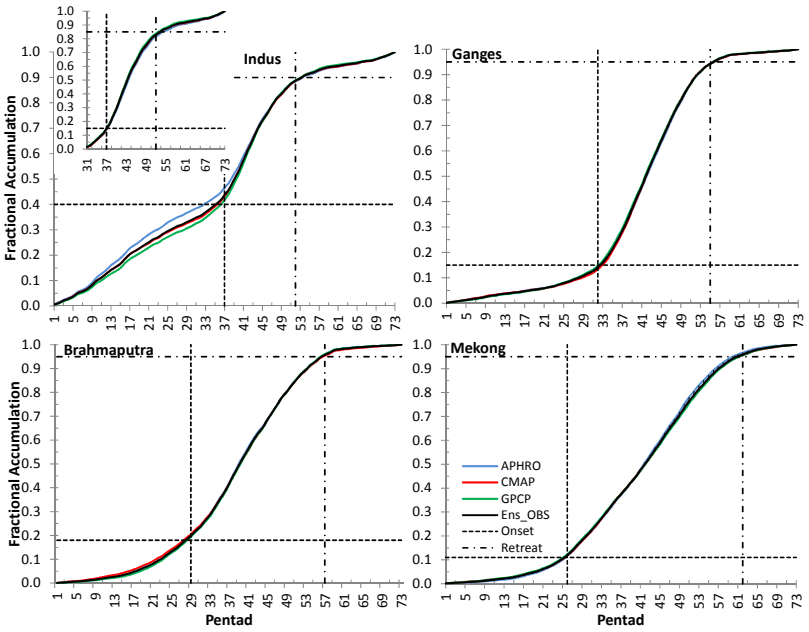

Figure 3. Fractional accumulated pentad precipitation from the observational datasets of GPCP, CMAP and APHRO along with their ensemble mean for Indus, Ganges, Brahmaputra and Mekong basins. Note: the pentads corresponding to realistic timings of monsoon onset and retreat timings around the middle of each basins are indicated with dashed lines. For Indus, the inset shows the fractional accumulation excluding January to May period of WPR.

Since RFA slope is only a measure of precipitation concentration during the active monsoon duration, it cannot analyze the seasonality of whole MPR. Moreover, the given monsoonal metrics (onset/retreat timings and RFA slope) cannot be equally applied to a year-round intermittent WPR. Therefore, a self-defining measure of the seasonality of overall precipitation regime is applied here, which is called the seasonality index (SI). The SI is multiplicative of the precipitation and the Kullback-Leibler distance [26] or the information-theory based relative entropy (RE) [15]. The RE represents the extent of precipitation concentration within a precipitation regime by quantifying the total divergence of the actual precipitation distribution from its uniform distribution [16,27]. Owing to the additive property of RE, its calculation is possible on a sub-seasonal scale [20], thus, it has been calculated separately for WPR and MPR in addition to the annual period. To calculate RE, first the fractional precipitation, $\pi_{i,x}$, at each grid cell, x, was computed for each pentad, i, of the considered period within a year using Equation (4):

$$\pi_{i,x} = \frac{p_{i,x}}{P_{t,x}} \quad where \quad i = 1...t \quad and \quad P_{t,x} = \sum_{i=1}^{t} p_{i,x} \tag{4}$$

where t represents the number of pentads within the annual period (73), MPR (36) and WPR (37) while $p_{i,x}$ represents the precipitation at pentad, i, and grid cell, x. Based upon π, RE was calculated on a sub-seasonal scale as:

$$RE_{t,x} = \sum_{i=1}^{t} \pi_{i,x} log_2(t\pi_{i,x}) \quad (5)$$

The highest $RE(= log_2 t)$ indicates that precipitation is concentrated within a shortest possible wet duration (here a single pentad) whereas its lowest value of zero represents a uniform precipitation distribution ($\pi_i = 1/t, i = 1...t$). The SI has been computed by multiplying the RE estimates with the total precipitation, $P_{t,x}$, normalized by its observed maximum, P_0:

$$SI_{t,x} = RE_{t,x} \frac{P_{t,x}}{P_0} \quad (6)$$

In the situations of either complete dryness or uniform precipitation distribution, SI is zero whereas it is maximum ($SI = log_2 t$) in the case of highest $RE(= log_2 t)$ for the year of P_0.

The seasonality indices have been distinctly applied to WPR, MPR and to annual course precipitation on yearly and climatological time scales (1961–2000). The spatial maps of the seasonality indices from CX-SA, CMIP5 and OBS individual datasets and their ensemble means have also been plotted and their regional scale performances have been summarized in the Taylor diagrams. Moreover, how these seasonality indices temporally evolve over the historical period (1971–2005) has been assessed by ascertaining the trend of their time series. This has been achieved by applying a widely used non-parametric Mann-Kendall test [55,56] for confirming the existence of a trend while its true slope has been estimated by the Sen's median slope approach [57,58].

5. Results and Discussions

The agreement amid OBS datasets on $\tilde{\prod}$ has been plotted in Figure 3 while Figure 4 presents such an agreement for those CX-SA experiments that are obtained by donwnscaling five CMIP5 experiments with a single RCM of CCAM, along with EC-EARTH-RCA4 and its driving GCM. The Figure 5 graphically summarizes the skill of two CX-SA experiments that are obtained by downscaling a single CMIP5 experiment using two different RCMs. The offsets of OBS, CX-SA and CMIP5 against GPCP and the added value/uncertainty of CX-SA relative to their driving CMIP5 experiments are summarized for the chosen skill metrics in Tables 2 and 3, respectively, and are graphically shown in Figure 6. The bold values in Tables 2 and 3 indicate the offsets that are statistically insignificant at 95% confidence level.

As for the indicators of the overall seasonality, the spatial maps of precipitation, RE and SI calculated from the ensemble means of OBS, CX-SA and CMIP5 have been shown in Figure 7 while the spatial maps from the individual dataset are shown in Figures 8–10 for WPR, MPR and annual scale precipitation, respectively. The spatial scale performance of all datasets have been summarized in the Taylor diagram (Figure 11). The agreements on the direction of temporal evolution of the seasonality indices and its significance amid OBS, CX-SA and CMIP5 ensembles are shown in Figure 12.

5.1. Statistical Properties of Monsoonal Precipitation Regime

As for the seasonal cycle of precipitation and its annual total, APHRO and GPCP feature a better agreement for Ganges and Brahmaputra but a weak agreement for relatively distant basins of Indus and Mekong. The CMAP underestimates precipitation for all basins relative to GPCP, and for Ganges and Brahmaputra relative to APHRO. As compared to OBS datasets considered here, the CRU (Climate Research Unit) observational dataset even suggests higher annual precipitation for the study basins, which is 415, 1125, 1350 and 1550 mm·yr^{-1} for Indus, Ganges, Brahmaputra and Mekong, respectively [5]. The differences amid OBS datasets mainly arise during the peak monsoon season (not shown).

The CX-SA and their driving CMIP5 experiments feature large scatter of their simulated annual precipitation, substantially overestimating the observed precipitation for Indus, Ganges and Brahmaputra (not shown). Only exceptions are EC-EARTH-RCA4 and MPI-ESM-LR for Indus and CNRM-CM5 for Ganges. Recent analysis on the eleven CX-SA experiments over the Himalayan region has also reported high fidelity of EC-EARTH_RCA4 [59]. For Mekong, the most of CMIP5 experiments are very close to OBS, however, CX-SA experiments suggest a mixed response of under-/overestimation. It is noted that CX-SA experiments performed using the same RCM suggest similar magnitude of annual precipitation regardless of the differences amid their driving CMIP5 experiments. For instance, all the CCAM-downscaled experiments simulate the annual precipitation around 700, 1200, 2300, and 750 mm·yr^{-1} for Indus, Ganges, Brahmaputra and Mekong, regardless of the fact that their driving CMIP5 experiments simulate the annual precipitation scatter of 440–880, 1030–1470, 1720–2330 and 1310–1650 mm·yr^{-1}, respectively. This clearly indicates that the employed RCM either can considerably modulate the lateral boundary conditions or becomes completely insensitive to them [60–63]. Furthermore, the two REMO-downscaled CX-SA experiments also suggest similar amount of annual precipitation for all basins, increasing (decreasing) the wet biases for Indus, Ganges and Mekong (Brahmaputra). An RCA4-downscaled CX-SA experiment has reduced the wet bias for Indus and Brahmaputra but increased it for Ganges and Mekong. Such differences in the magnitude of precipitation amid the considered observational and simulated datasets can hinder the adequate assessment of evolution of seasonal cycle of precipitation and qualitative assessment of the overall seasonality of precipitation regimes; hence $\tilde{\prod}$ was computed (Figure 3).

The pentads that suggest the realistic timings of the climatological monsoon onset and retreat around the middle of each respective basin are indicated by the dashed lines in Figure 3. Such pentads for the onset timings are 37, 32, 29 and 26 for Indus, Ganges, Brahmaputra and Mekong, respectively. The fractional accumulation, $\tilde{\prod}_t$, given at the observed onset pentads, t, are taken as the relative thresholds for each basin to identify the onset pentads from CX-SA and CMIP5 experiments. Similar procedure was adopted for identifying the pentads of the monsoon retreat. Since Indus feature a bimodal precipitation distribution, its WPR can significantly influence the onset timings of MPR. Thus, the onset and retreat pentads for Indus are identified based on pentads 31 to 73. The identified relative thresholds for Indus, Ganges, Brahmaputra and Mekong are 0.15, 0.15, 0.18 and 0.11 for the monsoon onset timings while 0.85, 0.95, 0.95 and 0.95 for the monsoon retreat timings, respectively.

The Figure 3 depicts that besides differences in the magnitudes, OBS datasets exhibit a best agreement for the seasonal cycle of precipitation, and thus, for the climatological monsoonal onset and retreat timings and for the precipitation concentration during the active monsoon period (RFA slope). For instance, APHRO and CMAP feature insignificantly delayed (early) onset by 1–4 days for Indus, Ganges and Mekong (Brahmaputra) as well as insignificant underestimation (overestimation) of RFA slope mostly by up to 4% for Indus and Brahmaputra (Ganges and Mekong). Such insignificant offset amid CMAP and GPCP for the same skill metrics has also been reported for a slightly different analysis period of 1961–2000 [20]. Here, only APHRO suggests significant overestimation of RFA slope (by 5%) for Mekong. Nevertheless, the best agreement among OBS datasets suggests that any of these datasets can potentially serve as a reference for the analysis of seasonal cycle of precipitation and its overall seasonality. Here, the main focus has been given either to GPCP or to the OBS ensemble mean.

As for the onset timings, four CX-SA experiments (CNRM-CM5_CCAM, GFDL-CM3_CCAM, MPI-ESM-LR_CCAM and EC-EARTH_RCA4) suggest right timings for Indus (insignificant offset from OBS), bringing an added value to their driving CMIP5 experiments; the former three simulate an early onset by 9–18 days while the latter one simulates a delayed onset by 7 days, relative to their driving CMIP5 experiments (Figure 4, Table 2). For other basins, such an added value of CX-SA experiments has been seen only from EC-EARTH_RCA4 that suggests the realistic onset

timings for Ganges and Brahmaputra and slightly improved bias for Mekong. The performance assessment of the eleven CX-SA experiments over the Himalayan region has also reported higher skill of EC-EARTH_RCA4 [59]. Interestingly, those CX-SA experiments that are performed with the CCAM RCM always achieve the monsoon onset earlier than their driving CMIP5 experiments for all basins, whenever such an offset was statistically significant (Table 3). As a result, CCAM's early onset relative to driving CMIP5 experiments is not always realistic. For instance, CCSM4 suggests a delay of five days in the onset timing for Indus while ACCESS1-0 suggests the realistic timing. However, their downscaled CX-SA experiments consistently achieve the onset timings earlier by five days against OBS. Similarly, the monsoon onset timings realistically suggested by two CMIP5 experiments (CCSM4 and MPO-ESM-LR) for Ganges, Brahmaputra and Mekong have been achieved far earlier in their CCAM-downscaled CX-SA derivatives relative to OBS, indicating an added uncertainty—instead of value—of the CCAM RCM. Similar case has been observed for the rest of CCAM-downscaled CX-SA experiments that further distance their driving CMIP5 experiments from OBS. These findings are in agreement with likewise findings that a typical increase in precipitation from the fine resolution experiments [64] is neither always realistic nor necessarily outperforms the well tuned coarse resolution experiments [65]. Further, regardless of a diverse response of the CMIP5 experiments, the early monsoon onsets achieved by their CCAM-downscaled CX-SA experiments indicate that RCMs can substantially modulate the behavior of lateral boundary conditions—consistent with the earlier findings [60–63]. This is further evident from the fact that a single CMIP5 experiment that has been downscaled by different RCMs yield different results. For instance, MPI-ESM-LR and its REMO-downscaled invariant (MPI-ESM-LR_REMO) feature insignificant differences in the suggested onset timings for Indus, Ganges and Mekong and only a small offset for Brahmaputra. In contrast, such differences are significant for all basins when MPI-ESM-LR is downscaled with the CCAM RCM (MPI-ESM-LR_CCAM), which achieves the monsoon onset far earlier (Figure 5, Table 3).

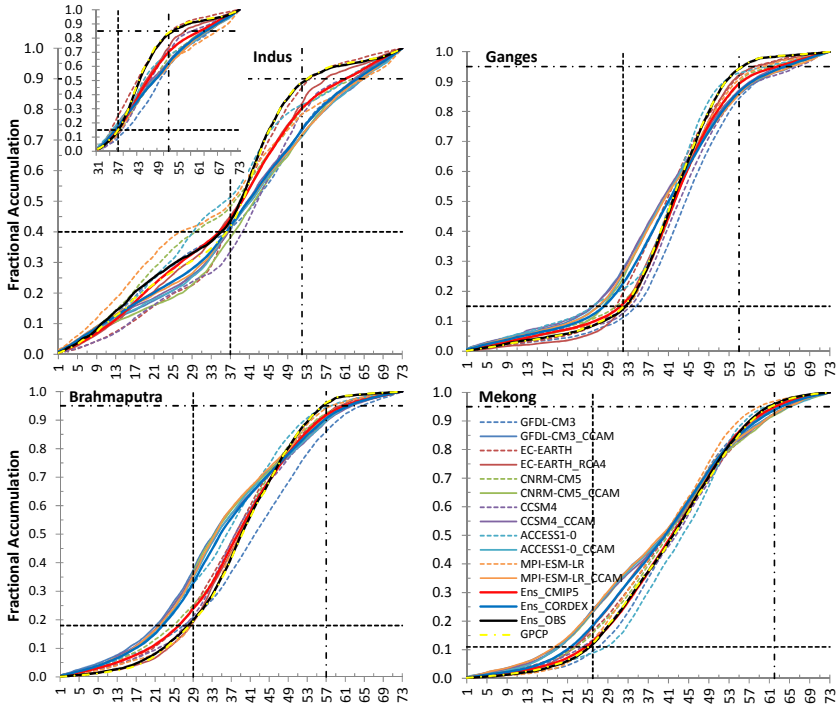

Figure 4. Fractional accumulation of precipitation; comparison of five CMIP5 experiments that are downscaled with a single RCM of CCAM as well as the EC-EARTH CMIP5 experiment downscaled with RCA4 RCM. The GPCP and the ensemble means of OBS, CX-SA and CMIP5 are also shown. For Indus, the inset shows the fractional accumulation excluding January to May period of WPR.

Table 2. First row: Observed onset pentads and RFA slopes from GPCP. Other rows: Offset of onset (in days) and RFA slope (in %) relative to GPCP. Note: Negative values indicate early onset or underestimated RFA slopes and vice versa. Bold values indicate statistically insignificant difference between the observed and the simulated climatological means.

CORDEX Models	Indus Onset	Indus Slope	Ganges Onset	Ganges Slope	Brahm Onset	Brahm Slope	Mekong Onset	Mekong Slope
GPCP	37	0.046	32	0.037	29	0.030	26	0.025
APHRO	**3**	**−10**	**2**	**2**	**−2**	**−2**	**2**	5
CMAP	**1**	**−7**	**4**	**4**	**−4**	**−3**	**2**	**1**
ACCESS1-0	**−1**	−40	−28	−19	−32	−21	18	18
ACCESS1-0_CCAM	−6	−46	−26	−36	−31	−35	−30	−22
CCSM4	9	−23	**3**	−28	**−6**	−23	−6	**−4**
CCSM4_CCAM	−5	−43	−33	−36	−34	−37	−30	−21
CNRM-CM5	6	−40	−10	−17	−18	−18	−12	−8
CNRM-CM5_CCAM	**−3**	−40	−19	−35	−33	−37	−31	−22
EC-EARTH	−9	−14	−7	−15	−12	−18	−17	−14
EC-EARTH_RCA4	**−2**	−27	**−1**	−10	**0**	−14	−15	−12
GFDL-CM3	15	−30	13	−22	−7	−24	9	7
GFDL-CM3_CCAM	**−3**	−45	−27	−37	−38	−37	−34	−22
MPI-ESM-LR	7	-45	**−2**	−14	**2**	−7	**−1**	5
MPI-ESM-LR_CCAM	**−3**	−45	−24	−37	−33	−33	−35	−22
MPI-ESM-LR_REMO	8	−35	−16	−32	−23	−27	−7	**−5**
MPI-ESM-LR_REMOi	8	−35	−16	−32	−22	−27	−7	−5

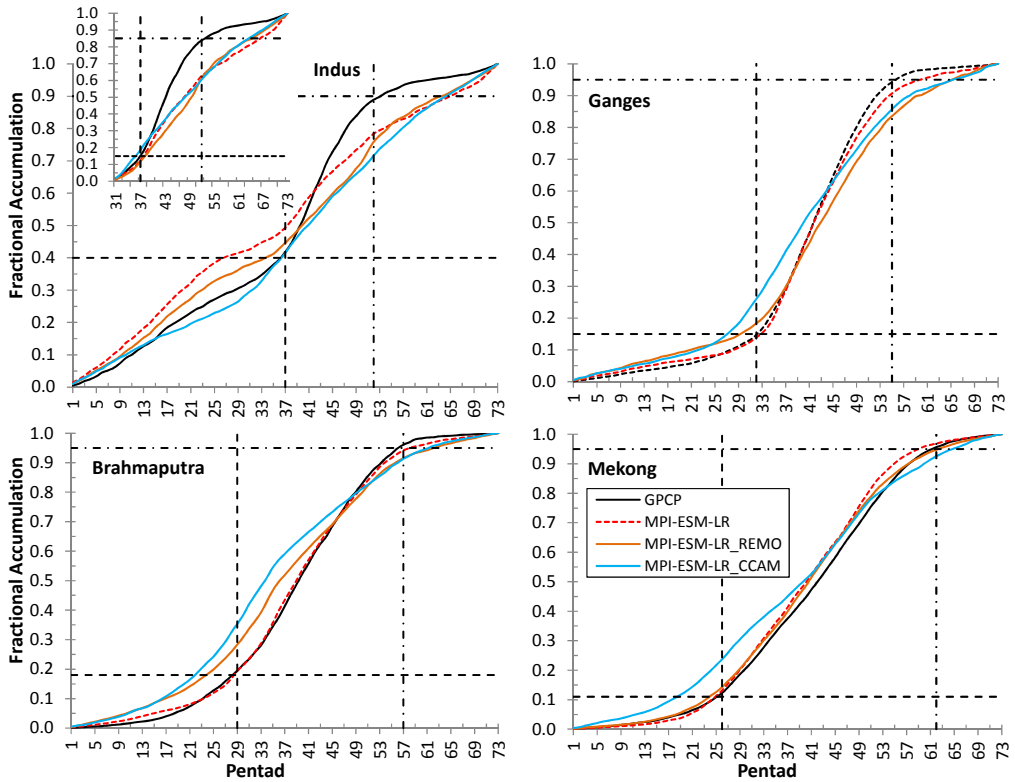

Figure 5. The fractional accumulation of precipitation; comparison of single MPI-ESM-LR CMIP5 model downsclaed with two different RCMs of REMO and CCAM. For Indus, the inset shows the fractional accumulation excluding January to May period of WPR.

Table 3. Offsets of onset (in days) and RFA slope (%) in CX-SA experiments relative to CMIP5 experiments. Note: Negative values indicate early onset or underestimated slopes and vice versa. Bold values indicate statistically insignificant difference between the climatological means of CX-SA and their CMIP5 driving datasets.

CORDEX Models	Indus Onset	Indus Slope	Ganges Onset	Ganges Slope	Brahm Onset	Brahm Slope	Mekong Onset	Mekong Slope
ACCESS1-0_CCAM	−5	**−8**	**3**	−21	**1**	−18	−48	−34
CCSM4_CCAM	−14	−26	−36	−12	−29	−17	−24	−18
CNRM-CM5_CCAM	−9	**−1**	−9	−21	−15	−22	−19	−15
EC-EARTH_RCA4	7	−15	6	**6**	11	**5**	**2**	**2**
GFDL-CM3_CCAM	−18	−21	−41	−20	−30	−17	−43	−27
MPI-ESM-LR_CCAM	−10	**0**	−22	−27	−35	−28	−34	−26
MPI-ESM-LR_REMO	**1**	18	**−14**	−22	−25	−22	**−5**	−9
MPI-ESM-LR_REMOi	**1**	18	**−14**	−22	−24	−22	**−5**	−10

As for the RFA slope, both CX-SA and CMIP5 experiments are unable to reproduce the extent of a sharp growth in the fractional accumulation, and thus, underestimate the RFA slope (Tables 2 and 3, Figure 6), which is higher in CX-SA than their driving CMIP5 experiments for all basins (except for EC-EARTH_RCA4). Such underestimation is due to the simulation of an extended active monsoon duration, such as, early onset and delayed retreat for Ganges and Brahmaputra, delayed retreat for Indus and early onset for Mekong. Amid CX-SA experiments, only EC-EARTH_RCA4 does not significantly alter the RFA slope biases of its driving GCM for Ganges, Brahmaputra and Mekong. Similarly, three CX-SA experiments (ACCESS1-0_CCAM, CNRM-CM5_CCAM and MPI-ESM-LR_CCAM) do not significantly change the RFA slope biases of their driving CMIP5 experiments for Indus (Tables 2 and 3, Figure 6).

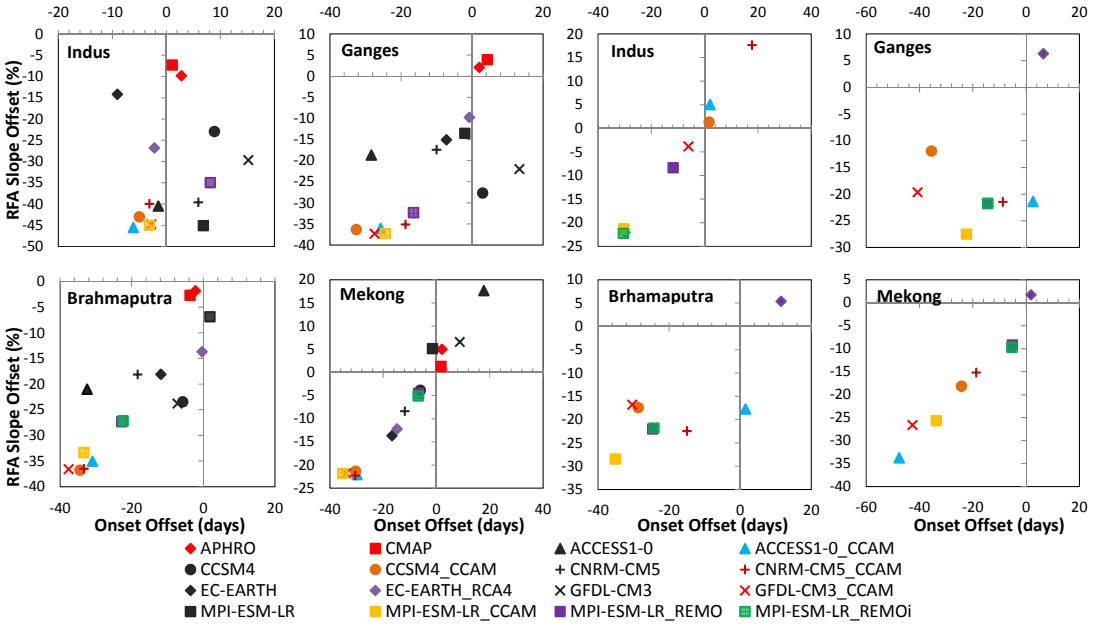

Figure 6. The offsets of rapid fractional accumulations (RFA) slopes against the suggested timings of the climatological monsoon onset from: all datasets relative to the GPCP observational dataset (left panel), the CX-SA relative to their driving CMIP5 datasets (right panel). Note: In the left panel, observations are shown in red whereas the driving CMIP5 GCMs (in black) and CX-SA (in different colors) are shown with the same marker shape. The positive values indicate a delayed onset or an overestimation of RFA slope while negative values indicate the opposite.

It to mention that the biases in the statistical properties of MPR and in the overall seasonal cycle of precipitation may remain uncorrected when (typically monthly) precipitation means are adjusted for bringing them closer to OBS [16]. Such uncorrected biases in the seasonality may severely affect the impact assessment results in terms of the timings of the hydrological processes and of the overall water availability.

5.2. Seasonality Indices of Overall Precipitation Regimes

The seasonality indices computed from the OBS ensemble mean, and relative to them, the biases of CX-SA and CMIP5 ensemble means for WPR, MPR and annual periods are plotted in Figure 7. In addition, the biases in the seasonality indices from all individual datasets are plotted in Figures 8–10 for MPR, WPR and annual period, respectively.

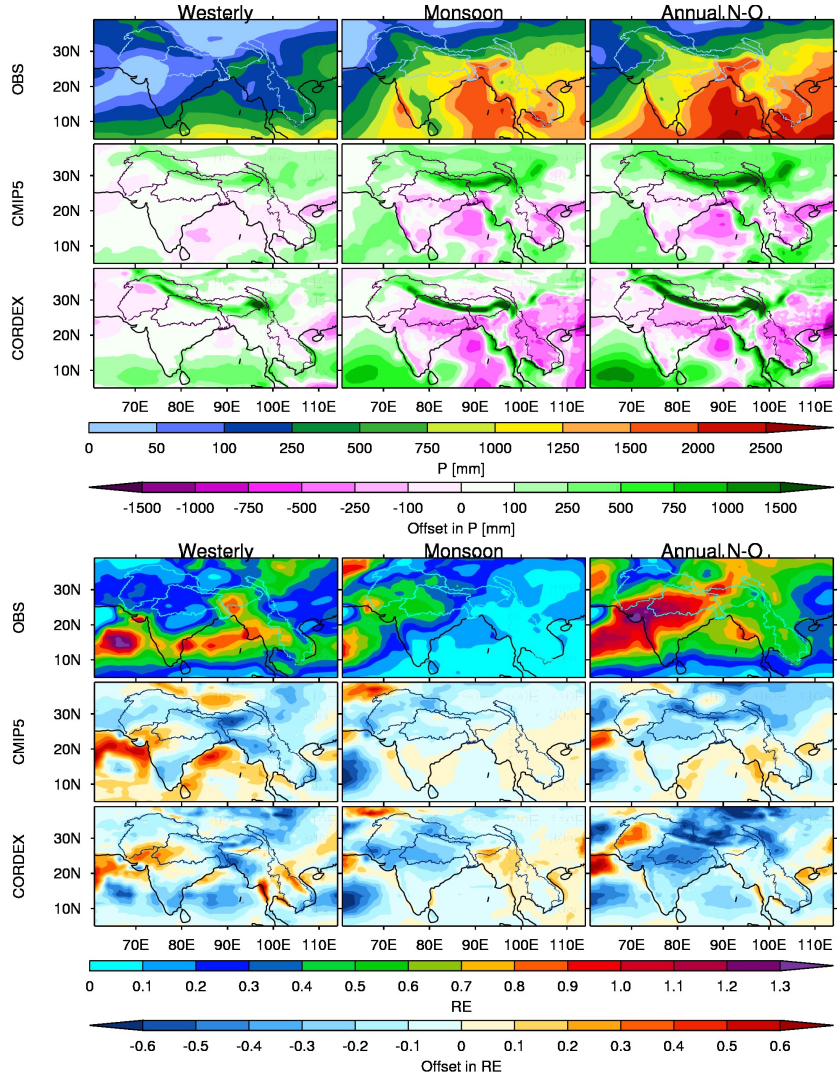

Figure 7. *Cont.*

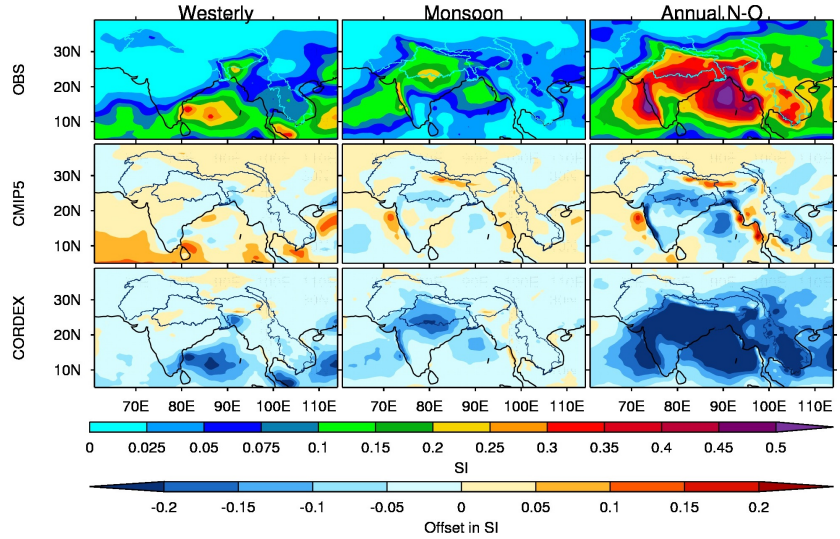

Figure 7. Top panel for precipitation, middle panel for relatively entropy (RE) and bottom panel for seasonality index (SI). The first row of each panel shows OBS P, RE and SI while the second and third rows show the offsets of CMIP5 and CX-SA ensemble means relative to OBS ensemble mean, respectively.

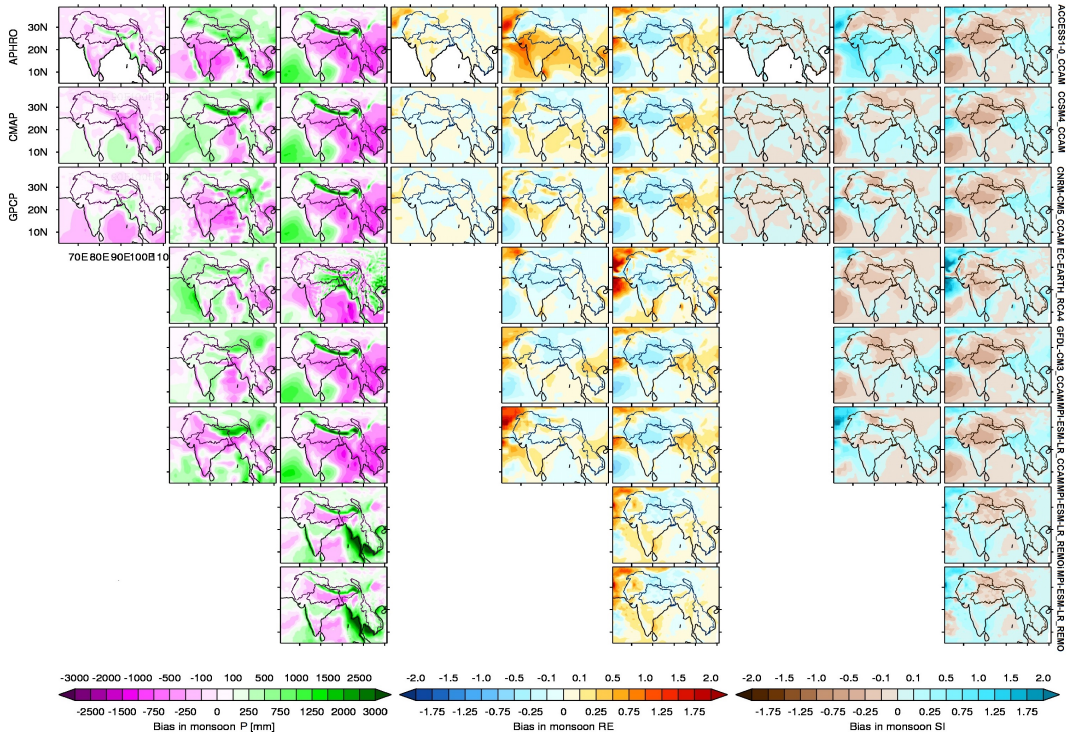

Figure 8. Offsets of precipitation (P), relative entropy (RE) and seasonality index (SI) for OBS, CMIP5 and CX-SA datasets from the OBS mean ensemble for the monsoonal precipitation regime.

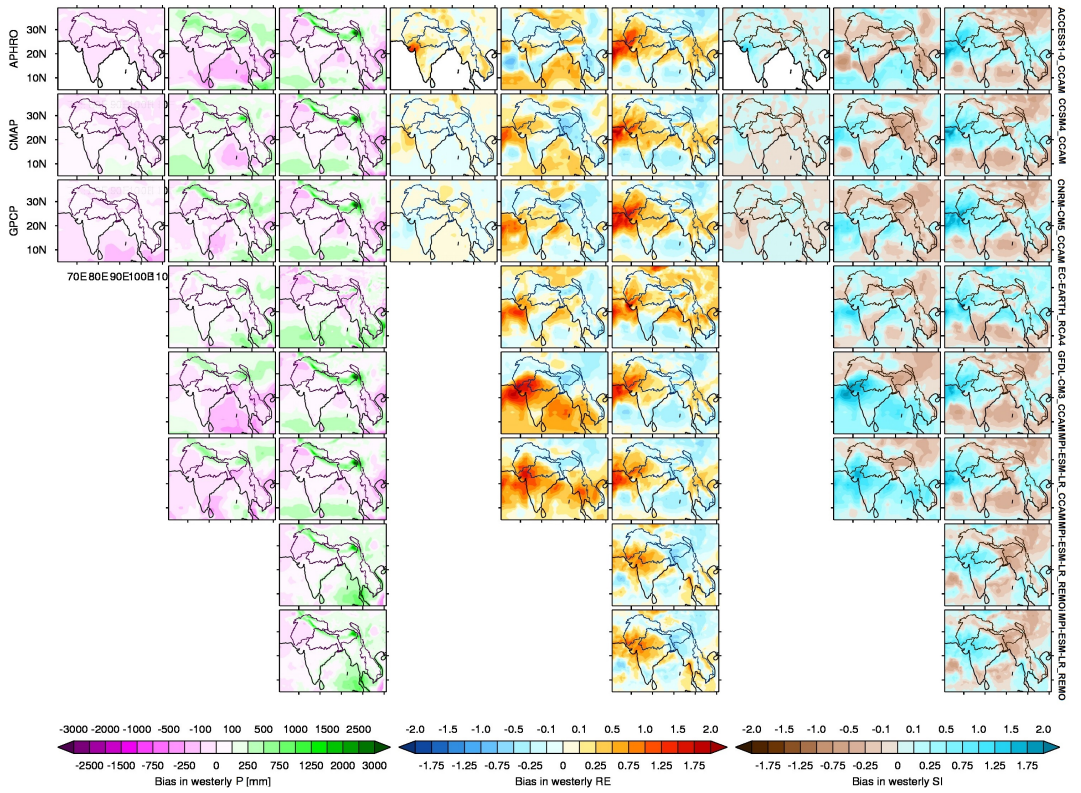

Figure 9. Same as Figure 8, but for the westerly precipitation regime.

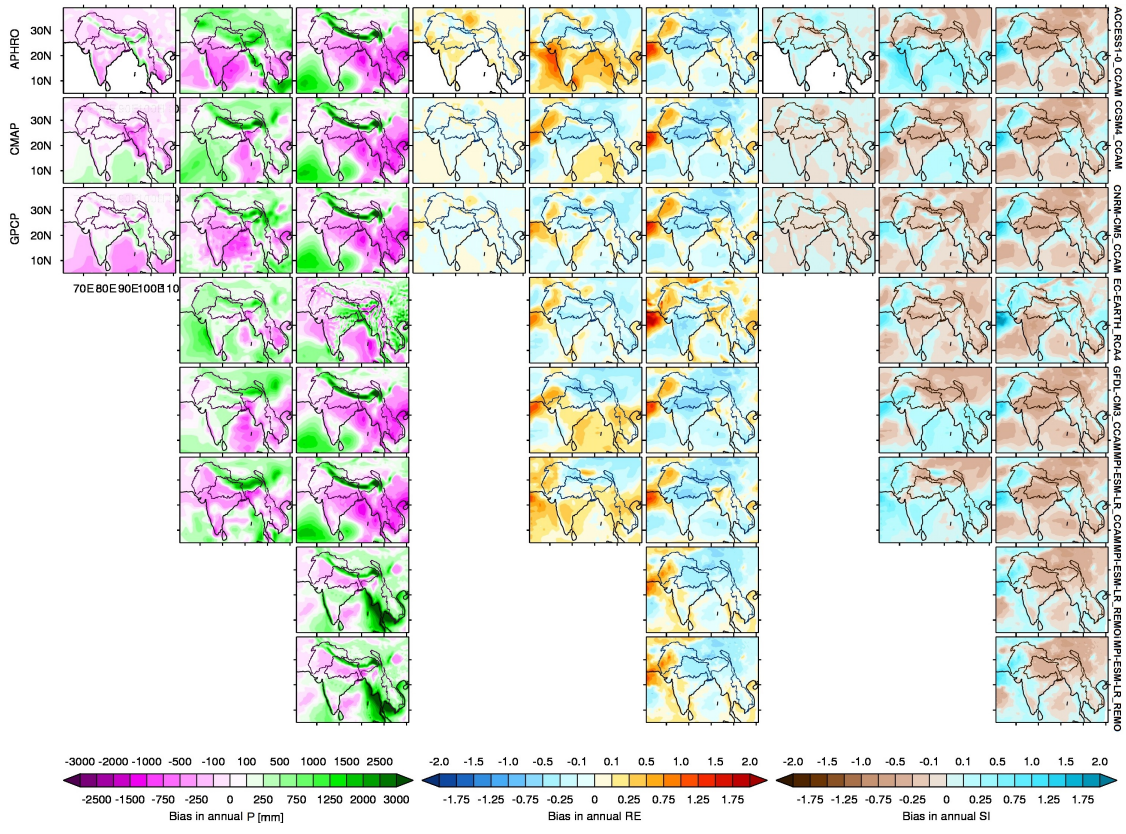

Figure 10. Same as Figure 8, but for the annual precipitation.

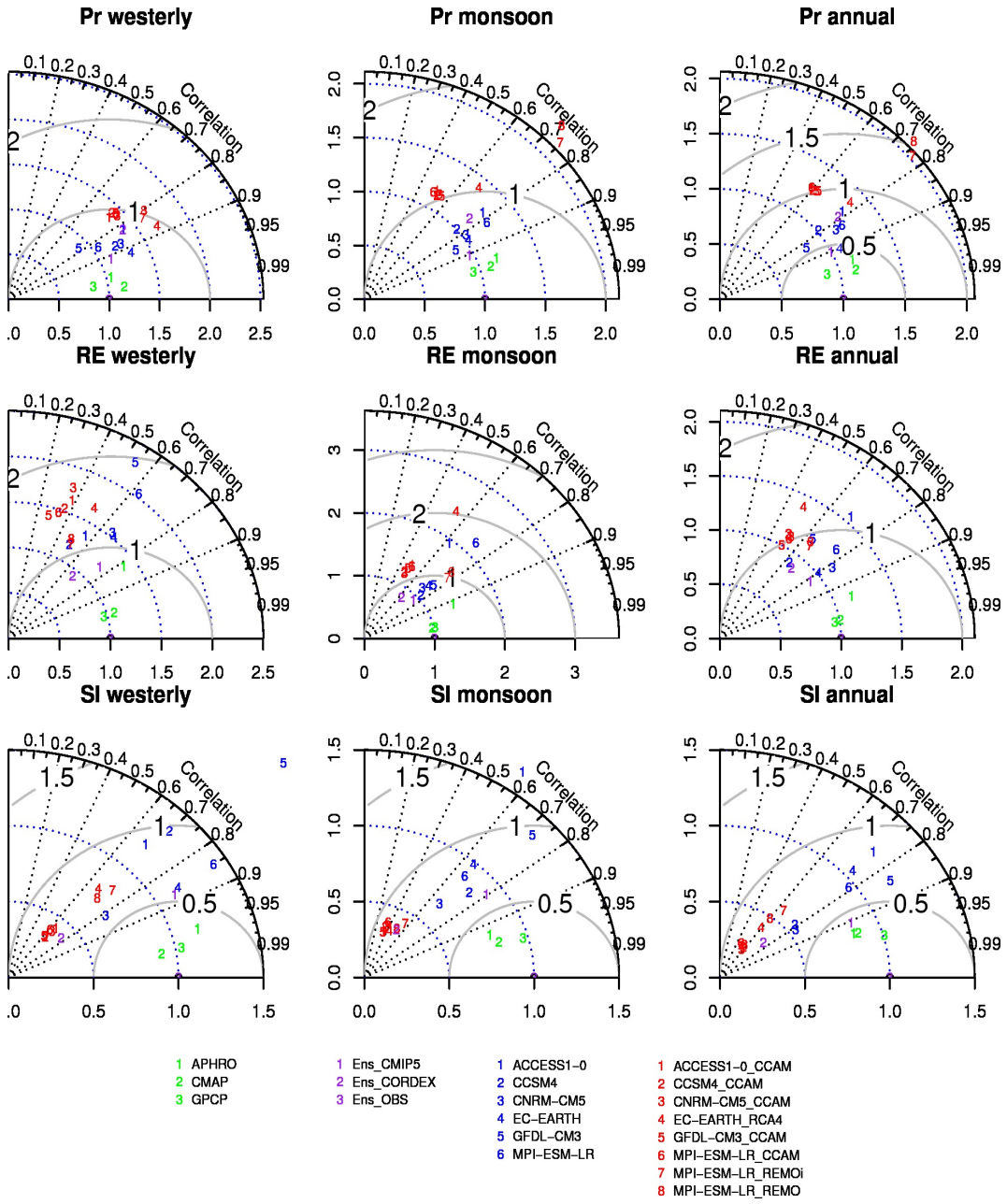

Figure 11. Columns left to right: Taylor Diagrams for the westerly precipitation regime (WPR), the monsoonal precipitation regime (MPR) and annual precipitation, respectively. Rows top to bottom: Taylor Diagrams for precipitation (P), relative entropy (RE) and seasonality index (SI), respectively. Note: The OBS ensemble mean has been taken as a reference.

5.2.1. Monsoonal Precipitation Regime

The OBS ensemble mean clearly identifies the real extent of the monsoonal domain (precipitation above 100 mm) and spots the areas of maximum precipitation as the western Ghats of India, Myanmar coast, Bay of Bengal, lower Mekong and Brahmaputra (Figure 7). Relative to the OBS ensemble mean, APHRO slightly overestimates precipitation along the Himalayan foothills, Myanmar coast and western Ghats of India while underestimates it over most of India, lower Mekong and lower Indus basins (Figure 8). The CMAP generally overestimates precipitation over the ocean but underestimates it over the land where such underestimation is higher over Myanmar, lower Brahmaputra and lower Ganges regions. The GPCP slightly overestimates precipitation over southern India, Myanmar

and lower Mekong. The substantial underestimation of CMAP precipitation over Myanmar region as compared to GPCP has also been reported earlier [20]. Overall, the pattern of precipitation distribution over the study domain is widely agreed between GPCP and CMAP, rather than between these datasets and APHRO (Figure 11).

As compared to the OBS ensemble mean, the CMIP5 ensemble mean overestimates precipitation over Himalayan region, Tibetan Plateau, Myanmar coast and Indus while underestimates over southern and central India, and lower Mekong. Such underestimation is consistent with the reports of a dry bias in CMIP5 experiments around 20°N [16,28,66]. Such quasi-systematic bias over the land region is likewise simulated over the Bay of Bengal, indicating an anomalous moisture advection to the high-altitude mountainous regions. Generally, a pattern of biases in the CMIP5 ensemble mean is intensified in the CX-SA ensemble mean, except for the overestimated precipitation over the Tibetan Plateau. The CMIP5 ensemble mean is quite close to the OBS ensemble mean, and thus, outperforms the CX-SA ensemble mean in terms of spatial patterns of precipitation across the study domain. When looking into the individual datasets, CMIP5 experiments exhibit a diverse skill. For instance, three CMIP5 experiments (ACCESS1-0, CNRM-CM5 and MPI-ESM-LR) feature a dry bias over the southern and central India while the rest are slightly biased positive. Moreover, a positive precipitation bias along the Himalayan foothills is only weakly agreed amid CMIP5 experiments. Similar case is observed over Indus where the half of CMIP5 experiments underestimate precipitation while the rest overestimate it. Over Indus, a diverse skill of CMIP5 experiments is subject to their: (1) inadequate representation of the western Karakoram topography 60°–80°E due to the adopted resolution [66–68]; (2) absence of irrigation schemes in the climate models [20,53,69], and; (3) consistent cold biases simulated in the sea surface temperature over the north Arabian sea [70–73]. Regardless of the diverse skill of CMIP5 experiments, the skill of their downscaled CX-SA experiments much depends upon the employed RCM since the CX-SA experiments that are obtained by downscaling five CMIP5 experiments (ACCESS1-0, CCSM4, CNRM-CM5, GFDL-CM3 and MPI-ESM-LR) using a single RCM of CCAM yield quite similar results, suggesting a substantial dry bias over the monsoon dominated plains and a wet bias along the Himalayan arc. Similarly, CX-SA experiments that are obtained by downscaling MPI-ESM-LR GCM with the REMO RCM are well agreed with each other but considerably differ to that obtained by downscaling the same GCM with the CCAM RCM. Further, the pattern of monsoonal precipitation biases for EC-EARTH GCM has been substantially changed when it has been downscaled by RCA4 RCM. These findings clearly indicate that RCMs can considerably alter the signal of driving datasets over the study region [60,62]. Consistent findings are reported for the West African Monsoon region, where RCMs are unable to systematically and homogeneously improve the biases of their driving GCMs in the simulated seasonal cycle of precipitation, indicating a profound role of RCMs' adopted internal physics, soil-moisture feedbacks and convective closures [63,74,75].

In contrast to the uniform overestimation of basin-integrated precipitation by CX-SA and CMIP5 experiments, the spatial maps (Figures 7 and 8) clearly suggest a dry bias over the monsoon dominated plains but a wet bias over the elevated regions of Himalayan ranges and Tibetan Plateau. Such dry and wet biases are greater in CX-SA experiments than in CMIP5 experiments. Analysis of precipitation characteristics from the eleven CX-SA experiments over the Himalayan region likewise suggests a wet (dry) bias over the Himalayan region (plains) [59]. Earlier studies have also reported a consistent wet bias over the Himalayan region from the vintage to the present-day GCMs [76,77], as well as, from their dynamically downscaled derivatives, including CX-SA experiments [60,62,78–82]. Such consistent wet bias may relate to the systematic bias of CMIP5 experiments in simulating unrealistically high convective precipitation [83]. Further, a greater wet bias in CX-SA experiments may subject to an improved representation of the regional topography at the adopted finer resolution (0.44°) that leads to the enhanced orographic precipitation. It is to noted that spatially explicit dry/wet biases have further biased the computation of the seasonality indices as well as the identification of the monsoonal domain.

The RE from the OBS ensemble mean is highest over the central and northwest India (Ganges), and over the lower Indus, indicating a shortest possible wet duration over there (Figure 7). A positive southeast-northwest gradient in the observed RE indicates additional sensitivity of Indus and Ganges to the active monsoon duration and to the total amount of precipitation received within such duration. Relative to the OBS ensemble mean RE, the CMIP5 ensemble mean slightly overestimate RE over Mekong and Myanmar (wet duration shorter than observed) but underestimate RE over Indus and Ganges (extended wet duration). Such pattern of RE bias is more prominent from the CX-SA ensemble mean RE. From OBS and CMIP5 individual datasets, biases in RE correspond well to the biases in precipitation; a dry bias leads to higher concentration of precipitation or shorter wet duration (overestimated RE) and vice versa (Figure 8). Interestingly, though dry (wet) biases for CX-SA individual datasets generally correspond well to the overestimation (underestimation) of RE over Mekong and Myanmar region (Himalayan arc), however such case is not observed over central India, Ganges and lower Indus, where regardless of a dry bias, RE is underestimated (extended wet duration or lower concentration of precipitation). The spatial pattern of RE from the most of CMIP5 experiments is well agreed with OBS. In contrast, featuring a better agreement with each other, CX-SA experiments are farther from OBS.

The OBS ensemble mean suggests the highest seasonality (SI estimates) over upper Indus, Ganges (or central India) and over the western Ghats while the lowest seasonality over lower Mekong, southern India and non-monsoonal region. The most of CMIP5 experiments and the ensemble mean underestimate SI over the regions of highest observed seasonality but overestimate SI over the regions of lowest observed seasonality. Though CX-SA ensemble mean uniformly underestimates SI across the study domain, such underestimation is highest over the regions of highest observed seasonality but lowest elsewhere. Such pattern is also well agreed amid the individual CX-SA experiments. The OBS ensemble mean SI yields a real extent of MPR (SI $\geq$ 0.025) and the seasonality hotspots, which are the central India and the western Ghats. Relative to OBS, the CMIP5 ensemble mean shows a positive bias in SI estimates over the most of Mekong, Myanmar, Himalayan range and Tibetan Plateau (owing to dry bias and overestimated RE) while a negative bias in SI over the central India (lower Ganges), upper Indus and western Ghats (owing to underestimated RE). The CX-SA ensemble mean, however, generally underestimates SI across the domain, which is highest over the central India due to the extended wet period. The individual CMIP5 experiments differ with each other on the pattern of SI biases. In contrast, CX-SA experiments largely agree on the underestimation of SI over the elevated regions (Himalaya and Tibetan Plateau), and central and northwest India while on the overestimation of SI over the rest of land regions. The CMIP5 experiments in general and EC-EARTH in particular agree well with OBS in terms of SI as compared to CX-SA experiments.

5.2.2. Westerly Precipitation Regime

As for precipitation, the OBS ensemble mean suggests the maximum precipitation over the upper Indus, Brahmaputra and lower Mekong as well as over the most of east China and the oceanic region (Figure 7). Against the OBS ensemble mean, GPCP and CMAP datasets feature a minute dry bias across the study domain (Figure 9). Relative to OBS, the CMIP5 ensemble mean suggests a substantial wet bias over the Himalayan ranges, despite of a minute dry bias over the rest of domain. In fact, such wet bias over the Himalayan ranges has been simulated by all CMIP5 experiments, except by EC-EARTH, which simulating almost right magnitude of precipitation and its spatial distribution, outperforms all CMIP5 and CX-SA experiments. In contrast to the rest of CMIP5 experiments, CCSM4 simulates a wet bias over Ganges and over southern and central India while three models (ACCESS1-0, GFDL-CM3 and MPI-ESM-LR) suggest a stronger dry bias over Myanmar and Mekong regions. Interestingly, the CX-SA ensemble mean suggests even stronger wet biases over the Himalayan ranges than CMIP5 experiments, which is supported by all individual experiments, except by EC-EARTH-RCA4. These results are in agreement with the reports of substantial wet bias in

CX-SA experiments over the high-altitude Himalayan regions [59] and during the winter season [84]. Further, all CX-SA experiments feature slightly higher dry bias over lower Indus basin. As noted before, the spatial scale performance has been found quite similar in the five CX-SA experiments that are downscaled with the single RCM of CCAM, besides differences in their driving CMIP5 experiments (Figures 9 and 11). Two CX-SA experiments downscaling the MPI-ESM-LR CMIP5 experiment using two different RCMs of CCAM and REMO, mainly differ on the wet/dry biases over Myanmar and lower Mekong regions.

The RE estimates from the OBS ensemble mean are maximum over the southern India, Myanmar, Mekong and Brahmaputra, indicating that these regions experience a shortest possible wet duration under WPR. On the other hand, the longest possible wet duration (lowest RE) is observed over the parts of central India, upper Brahmaputra and over the most of upper Indus basin. As compared to GPCP and CMAP, APHRO suggests higher RE over Thar and Rajhistan deserts, and over Myanmar and lower Mekong regions, owing to its dry bias therein. The CMIP5 and CX-SA ensemble means simulate positive biases over the driest regions (higher RE over deserts) and negative biases over the rest of the land regions. The positive RE bias over the desert region is relatively higher in two CMIP5 experiments (GFDL-CM3 and MPI-ESM-LR) and in all CCAM-downscaled CX-SA experiments, exhibiting their low fidelity relative to the rest of experiments (Figure 11).

The OBS ensemble mean suggests a highest seasonality (SI estimates) over Brahmaputra due to the fact that a shortest wet duration (highest RE) has been observed there. In contrast, the seasonality is low over the most of southern India, Myanmar and Mekong besides high RE because the overall incident precipitation is low over these regions. Relative to GPCP and CMAP, APHRO suggests a higher seasonality over the most of study domain, owing to its relative dry bias and positive RE bias. The CMIP5 ensemble mean overestimates SI over the deserts and central India (Ganges) while underestimates it over the rest of the land region (basins) where such a pattern is dominated by four CMIP5 experiments (ACCESS1-0, CCSM4, CNRM-CM5 and EC-EARTH). The rest of two CMIP5 experiments (GFDL-CM3 and MPI-ESM-LR) underestimate SI over the upper parts of the study basins while overestimate it over the rest of the study domain. Again, EC-EARTH outperforms in terms of its spatial scale agreement with OBS. The CX-SA ensemble mean slightly underestimates SI across the study domain. The individual CCAM-downscaled experiments exhibit a slight underestimation over the Himalayan and Tibetan regions while the REMO-downscaled experiments additionally underestimate SI over the Myanmar and Brahmaputra.

5.2.3. Overall Precipitation Regime (Annual)

APHRO slightly overestimates the annual precipitation relative to the OBS ensemble mean over Himalayan ranges while CMAP features a dry bias over Myanmar region. The CMIP5 ensemble mean features a clear dry bias over the lower Mekong (dominated by all individual experiments, except CCSM4) and over the southern and central India (dominated by ACCESS1-0, CNRM-CM5 and MPI-ESM-LR). Moreover, a wet bias over the Himalayan ranges and Tibetan Plateau (Indus, Brahmaputra, upper Ganges and upper Mekong) is well agreed amid CMIP5 individual experiments, and thus, with their ensemble mean. The CX-SA experiments also agree well with each other and with their ensemble mean on (even a stronger) wet bias over Himalaya and mostly on dry bias over the rest of the land region; a pattern generally dominated by the biases in MPR.

The OBS ensemble mean RE shows the annual scale concentration of precipitation (or wet/dry duration) and its gradient across the study domain. From the individual observations, APHRO suggests a slightly shorter annual wet duration while CMAP and GPCP suggest the opposite. The CMIP5 ensemble mean RE is underestimated over the most of the study domain with a few exceptions. Such biases are higher in magnitude for CX-SA ensemble mean. All CMIP5 experiments except ACCESS1-0 simulate a shorter wet duration for Indus while three experiments (ACCESS1-0, GFDL-CM3 and MPI-ESM-LR) simulate the same for the land region of lower half

of study domain. The rest of CMIP5 experiments generally simulate an extended wet duration (precipitation concentration lower than observed).

It is noted that the real extent of the monsoonal domain is more clearly visible from the OBS ensemble mean SI ($\geq$0.11) where the regions of highest observed seasonality are the western Ghats, followed by central India, lower Ganges and Brahmaputra. The same threshold has also been reported earlier for identifying the spatial extent of MPR from the pentad precipitation [20]. On a monthly temporal resolution, such SI based threshold was reported as $\geq$0.05 [16]. These findings suggest that besides the coarse-grained resolution, the SI-based thresholds yield realistic spatial extent of MPR, and that, these thresholds can be applied to assess the future changes in the spatial domains of MPR under warmer climates. Against the OBS ensemble mean, the seasonality estimates from the CMIP5 ensemble mean are substantially underestimated over lower Ganges, lower Mekong and western Ghats, slightly underestimated over the most of India, eastern China and upper Indus while overestimated elsewhere. The underestimated CMIP5 ensemble mean SI over India, lower Mekong and lower Ganges is dominated by three experiments (CCSM4, CNRM-CM5 and EC-EARTH), and over Indus by ACCESS1-0. The CX-SA ensemble mean substantially underestimates the seasonality over the most of the study domain, where such pattern is well agreed amid the individual experiments. With a modest intermodel agreement, CMIP5 experiments generally outperform their downscaled CX-SA experiments, which though well agreed with each other are farther from OBS in terms of spatial patterns of SI.

5.3. Trend Changes in the Seasonality Indices of Precipitation Regimes

In view of the limited fidelity of CMIP5 and CX-SA experiments in terms of reproducing the observed seasonality on a climatological scale, an assessment of temporal changes in the seasonality indices has been presented qualitatively. In this regard, trend direction and its significance from each individual dataset have been summarized in a trend agreement for each ensemble (OBS, CMIP5 and CX-SA). The trend agreement has been computed as the total number of members within a particular ensemble that agree on a positive trend minus the number of members featuring a negative trend (Figure 12). The locations, where the number of statistically significant positive trends (at 90% significance level) were higher than the number of significant negative trends, are identified with the stippling of hollow circles while the location featuring the opposite case are indicated with the stippling of filled circles.

5.3.1. Monsoonal Precipitation Regime

The OBS ensemble exhibits a well-agreed significant rising trend in precipitation between 80° and 90°E (covering Tibetan Plateau, Brahmaputra and eastern Ganges) and over Mekong while mostly an insignificant falling trend over lower Indus, northwest India and over parts of China. Surprisingly, the observed decreasing trend in All-India precipitation [12,85,86] is not apparent from OBS datasets; only statistically insignificant trend is observed over central and northwest India. This may result from the integration of precipitation over MPR rather than over the typical monsoon period of June–September. When compared to OBS, CMIP5 and CX-SA ensembles exhibit quite a different pattern of agreement on the direction of change in precipitation and its significance. The CMIP5 experiments agree on a significant positive precipitation change over the most of the monsoon dominated plains except for eastern Ganges, Brahmaputra and eastern China. This rising trend in the simulated precipitation over India, being consistently reported by various studies [12,85,86], have been linked to the inability of CMIP5 models in realistically representing the relationship of the monsoon weakening with the: (1) strengthening of cyclonic formation in tropical west pacific ocean; (2) warming of southern Indian ocean [12]. The contrasting rising precipitation trend may also be due to the fact that the most of CMIP5 models simulate unrealistically high local convective precipitation [83]. In contrast to CMIP5, the CX-SA ensemble however suggests a

significant decreasing precipitation trend over southern and central India. The CX-SA experiments further differ from CMIP5 in terms of a sporadic positive trend over Ganges and upper Indus.

As for RE, OBS ensemble exhibits a decreasing trend over the Tibetan Plateau and over the monsoon dominated plains, where such trends are significant over all study basins, except Ganges. A significant rise in OBS RE has been observed over eastern China, which is consistent with both CMIP5 and CX-SA ensembles. For the rest of the study domain, CMIP5 ensemble either does not suggest a clear agreement or a signal of change is found statistically insignificant. In contrast, CX-SA experiments are well agreed on a rise in RE over lower Mekong but only sporadically over Myanmar and upper Indus.

Owing to changes in OBS precipitation and RE, there is a clear signal of change in OBS SI, suggesting a significant decrease over the most of Indus, western Ghats, Myanmar, lower Mekong and eastern Tibetan Plateau while a significant increase over eastern China. In contrast, CMIP5 and CX-SA exhibit quite noisy patterns of the direction change agreement, which are further only sporadically significant. Nevertheless, CMIP5 and CX-SA are consistent with each other on a rise in the seasonality over lower Mekong, Himalayan range, upper Indus and for parts of eastern China and Tibetan Plateau.

5.3.2. Westerly Precipitation Regime

In Figure 12, the most of OBS datasets agree on a significant increasing trend of precipitation over lower Mekong, Tibetan Plateau and surrounding region as well as over western Brahmaputra and eastern Ganges (along 90°E). There is also an evidence of a significant rising precipitation over northwest Karakoram (Hunza sub-basin within Indus) as observed from the novel high-altitude station observations [87]. This may suggest the suitability of gridded observations for ascertaining qualitative changes in WPR. For the rest of the land region, precipitation features a decreasing tendency, which is significant over the parts of Indus and Myanmar region. In contrast, the most of CMIP5 experiments suggest an increasing precipitation over southern India and Tibetan Plateau but a decreasing precipitation over all study basins, where such a decrease has also been projected by the CMIP3 experiments [22]. Further differing from driving CMIP5 experiments, CX-SA experiments agree on a decreasing precipitation over the most of the study domain except upper Indus and parts of Ganges or Himalayan range. Such pattern of CX-SA is consistent with OBS datasets.

The OBS ensemble mostly agrees on a significantly rising precipitation concentration (RE) over the whole Indus and parts of central India while on a significantly decreasing RE over lower Mekong. Whereas, the most of CMIP5 experiments exhibit a significantly rising RE trend over the elevated regions and eastern China but no clear agreement on the sign and significance of RE change over the land region, particularly over the southern India where CMIP5 ensemble simulates a significant rising precipitation trend. The CX-SA pattern of agreement on RE change matches quite well with that of OBS RE, such as, a significant rising trend over Indus, western Tibetan plateau and eastern China while a significant falling trend over central India and lower Mekong.

The OBS SI is going to be reduced over Indus, Myanmar and most of India while it will increase over lower Mekong and parts of Tibetan Plateau, clearly following the signs of precipitation trends. In contrast, the most of CMIP5 experiments agree well on an insignificant negative trend in SI between 20° and 30°N but on a significant positive trend below and above this latitudinal range. Such pattern of SI changes is consistent with the signs of trends in the simulated precipitation. The most of CX-SA experiments agree well on a significant decreasing SI over the most of India and lower Mekong but on a significant increasing SI over Himalayan range and western Tibetan Plateau.

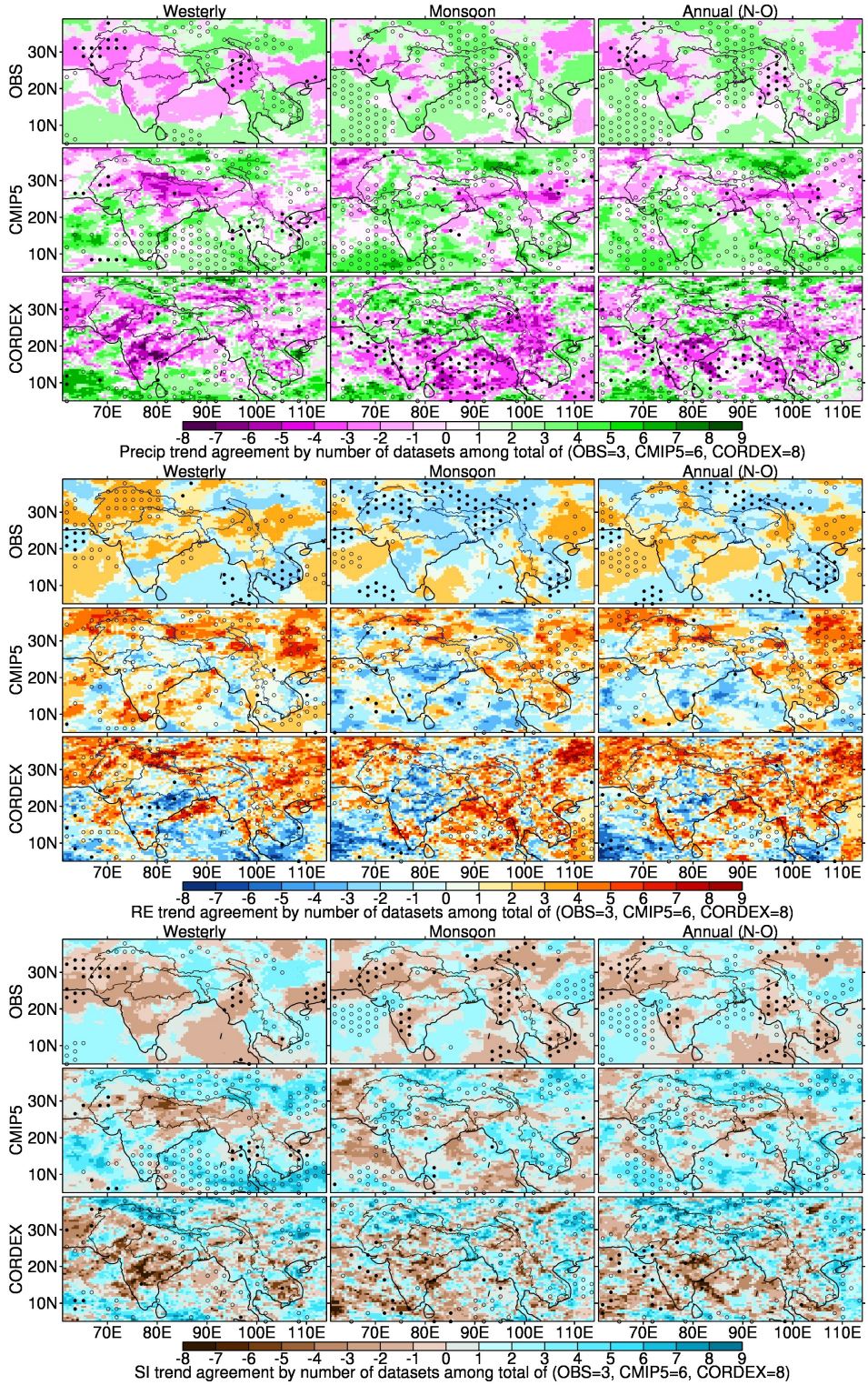

Figure 12. Agreement on trend direction and its significance: Panel top to bottom: precipitation (P), relative entropy (RE) and seasonality index (SI), Row top to bottom: OBS, CMIP5 and CX-SA ensembles. Agreement is computed as the total number of ensemble members agreeing on the positive direction minus those exhibiting the negative direction. The hollow circles show where the statistically significant positive trends (at 90% significance level) are higher in number than the significant negative trends amid ensemble members while the filled circles show the opposite.

5.3.3. Overall Precipitation Regime (Annual)

A pattern of agreement for temporal changes in the annual precipitation is not very much different from that of MPR for OBS, CMIP5 and CX-SA ensembles. In case of annual RE, OBS ensemble exhibits less area under significant changes as only Tibetan Plateau and lower Mekong feature a significant falling trend while eastern China features a significant rising trend. This pattern is mostly consistent with MPR, and to some extent, with WPR. The rest of regions that feature significant (positive) changes for one of the precipitation regime (WPR/MPR) observe an opposite sign of change (negative) in the other and vice versa. The CMIP5 and CX-SA agree with each other and with OBS on a rise in RE over the eastern China and only with each other on a rise over Brahmaputra, upper Indus and Mekong. The pattern of agreement on change in the annual OBS SI is dominated by that of MPR. There is a more clear signal of significant rising trend in OBS SI for the region along 90°E and over the Tibetan Plateau, which is somewhat consistent with CMIP5 and CX-SA ensembles. For the rest of regions, CMIP5 and CX-SA ensembles suggest an opposite signal of SI change as compared to OBS. The CMIP5 ensemble agree on a rising trend in the seasonality over the most of study domain whereas CX-SA ensemble mostly suggests a rising (falling) trend over northern (southern) parts.

6. Summary and Conclusions

The gridded observations, either considered here or elsewhere, feature a diverse skill across the Himalayan watersheds and over other parts of the study region, featuring considerable differences in their suggested magnitude of seasonal and annual precipitation, which are mainly observed during the peak monsoon season. However, besides differences in the magnitudes, the considered observations reveal a best agreement (statistically insignificant differences) on the seasonal cycle of precipitation, and thus, on the climatological monsoonal onset and retreat timings, concentration of precipitation during the active monsoon duration and overall seasonality of WPR, MPR and annual precipitation. Such a best agreement suggests that any of these observations can potentially serve as a reference dataset for analyzing the annual cycle of precipitation and its overall seasonality. Surprisingly, previously reported post-1950 all-India falling precipitation trend is not apparent from the individual OBS ensemble members; only statistically insignificant trend is observed over central and northwest India.

For the western basins (Indus, Ganges and Brahmaputra), CX-SA experiments feature a greater wet bias relative to their driving CMIP5 experiments, against OBS. For Mekong, CX-SA experiments exhibit a mixed response as compared to their high fidelity driving CMIP5 experiments. The spatial maps suggest that the basin scale wet biases has resulted from a substantial wet bias simulated over the Himalayan and Tibetan regions (Indus, Brahmaputra, upper Ganges and upper Mekong) despite of a dry bias simulated over the monsoon dominated plains for WPR, MPR and annual precipitation. Such pattern of dry and wet biases has been intensified in CX-SA experiments compared to their driving CMIP5 experiments. The trend analysis for MPR reveals that the CMIP5 and CX-SA ensembles exhibit quite a different pattern of agreement on the direction of change in precipitation and its significance. In contrast to OBS, CMIP5 ensemble suggests an opposite trend of increasing precipitation over most of India and Myanmar region but decreasing precipitation over Brahmaputra and eastern Ganges. However, CX-SA ensemble exhibits some consistency with OBS, such as, a significant decreasing precipitation trend over southern and central India and over Myanmar region and an increasing precipitation trend over Brahmaputra and eastern Ganges. Similarly for WPR, CX-SA ensemble suggests a negative (though insignificant) precipitation trend across the study domain, which is consistent with OBS over southern India, Indus and Ganges but in disagreement with CMIP5 over southern India. For annual precipitation, trend pattern is largely dominated by that of MPR. Summarizing, the CMIP5 ensemble mean generally outperforms the CX-SA ensemble mean in terms of the spatial patterns and the magnitude of precipitation distribution across the study domain, except for trend changes.

As for the monsoon onset timings, four CX-SA experiments (CNRM-CM5_CCAM, GFDL-CM3_CCAM, MPI-ESM-LR_CCAM and EC-EARTH_RCA4) suggest right timings of the monsoon onset for Indus (insignificant offset from OBS), bringing an added value to those CMIP5 experiments whose performance was relatively poor for the basin. Interestingly, CX-SA experiments performed with CCAM RCM always achieve the monsoon onset far earlier and unrealistic than their driving CMIP5 experiments for all basins, whenever such an offset was found statistically significant. For the RFA slope, CX-SA and CMIP5 experiments are unable to reproduce the observed extent of sharp growth in the fractional accumulation, and thus, substantially underestimate the RFA slope. This has resulted from the simulation of an extended wet period by CMIP5 and CX-SA experiments relative to OBS—early onset and/or later retreat. Surprisingly, such underestimation of RFA slope is higher in CX-SA experiments than in their driving CMIP5 experiments for all basins (except for EC-EARTH_RCA4).

The spatial maps of MPR RE show its positive gradient from the southeast to the northwest of the study domain, implying a shortening of MPR duration north and northwestward. This indicates the additional sensitivity of the western basins (Indus and Ganges) to the active duration of MPR and to the magnitude of monsoonal precipitation, apart from the onset timings. Further, CX-SA experiments though feature a better agreement with OBS on the overall spatial patterns, however, these experiments substantially underestimate RE (simulate an extended wet duration) over the most of study domain, where such underestimation is higher in magnitude than that of the driving CMIP5 experiments and generally follows a pattern of precipitation biases with few exceptions; a dry bias may yield higher concentration of precipitation or shorter wet duration and vice versa. For WPR RE, the most of CX-SA and CMIP5 experiments additionally simulate a positive bias over the driest regions though the annual scale RE is generally underestimated. The trend analysis of the OBS RE suggests a significant decreasing trend over the study basins, Himalayan Range, Tibetan Plateau and southern and central India for MPR while mostly an increasing trend for WPR except over lower Mekong. The CX-SA and CMIP5 experiments suggest a rising WPR RE over upper Indus and eastern China and a falling MPR RE over central India while for the rest of regions both ensembles either do not suggest a clear agreement or their signal of change has been found insignificant.

As for MPR SI, the OBS ensemble mean suggests the highest seasonality (SI estimates) over upper Indus, Ganges (or central India) and over the western Ghats while the lowest seasonality over lower Mekong, southern India and non-monsoonal region. The most of CMIP5 experiments and the ensemble mean underestimate MPR SI over the regions of highest observed seasonality and overestimates it over the regions of lowest observed seasonality. Though CX-SA uniformly underestimates MPR SI across the study domain, such underestimation is highest over the regions of highest observed seasonality but lowest elsewhere, which is also well agreed amid the CX-SA individual experiments. For WPR, OBS SI is highest over Brahmaputra, followed by lower Mekong, and the lowest elsewhere. The CMIP5 ensemble mean overestimates WPR SI over the deserts and central India (Ganges) while underestimates it over the rest of the land region (basins) while the CX-SA ensemble mean slightly underestimates WPR SI across the whole study domain. The trend analysis suggests that the observed seasonality of MPR mostly features a decreasing trend over Indus, southwest India, eastern Tibetan Plateau, Myanmar and lower Mekong. The CMIP5 ensemble agree on a rising trend in the seasonality of MPR over the most of the study domain whereas CX-SA ensemble mostly suggests a rising (falling) trend over northern (southern) parts. The observed WPR SI features a decreasing trend over Indus, Ganges, Myanmar (Brahmaputra and Mekong and Tibetan Plateau). The most of CX-SA experiments agree well on a significantly increasing WPR SI over Himalayan range and western Tibetan Plateau but a significantly decreasing SI over the most of India and lower Mekong. Only a decreasing SI trend over India in CX-SA experiments and increasing SI trend over Mekong and Tibetan Plateau in CMIP5 experiments are consistent with OBS.

For the most of skill metrics, biases in CMIP5 experiments are simply intensified in their downscaled CX-SA experiments, indicating their added uncertainty. More interestingly, the overall

performance of those CX-SA experiments that have employed the same RCM of CCAM has been found quite similar, regardless of the skill of their driving CMIP5 experiments. Similarly, the two CX-SA datasets that are obtained by downscaling the MPI-ESM-LR GCM with the REMO RCM are well agreed with each other but considerably differ to that obtained by downscaling the same GCM with the CCAM RCM. These findings clearly indicate that RCMs can considerably alter the signal of driving datasets. These findings emphasize on improving the fidelity of RCMs in order to ensure the added value to their coarse resolution CMIP5 experiments. This requires the exploitation of RCMs' potential in terms of microphysics, resolutions and convective closures, and preferably, resolving the crucial fine scale processes, land-atmosphere interactions and feedback further down to their representative (meso-to-local) scales.

Acknowledgments: The author acknowledges the World Climate Research Programme's Working Groups on Coupled Modeling responsible for CMIP and on Regional Climate, former coordinating body of CORDEX, and the climate modeling groups for producing and making available their model outputs as listed in Table 2. For CMIP the U.S. Department of Energy's Program for Climate Model Diagnosis and Intercomparison provides coordinating support and led development of software infrastructure in partnership with the Global Organization for Earth System Science Portals. The author also acknowledges the support of the CliSAP/Cluster of excellence in the Integrated Climate System Analysis and Prediction (EXC 177), Universität Hamburg, funded through the German Science Foundation (DFG).

Conflicts of Interest: The author declares no conflict of interest.

References

1. IPCC. *Climate Change 2007: The Physical Science Basis: Working Group I Contribution to the Fourth Assessment Report of The Intergovernmental Panel on Climate Change*; Cambridge Universitiy Press: New York, NY, USA, 2007.
2. IPCC. *Climate Change 2013: The Physical Science Basis. Contribution of Working Group I to the Fifth Assessment Report of The Intergovernmental Panel on Climate Change*; Cambridge Universitiy Press: New York, NY, USA, 2013.
3. Mountain Research Initiative (MRI). Elevation-dependent warming in mountain regions of the world. *Nat. Clim. Chang.* **2015**, *5*, 424–430.
4. Hasson, S.; Gerlitz, L.; Schickhoff, U.; Scholten, T.; Böhner, J. Recent climate change over High Asia. In *Climate Change, Glacier Response, and Vegetation Dynamics in the Himalaya*; Springer International Publishing: Basel, Switzerland, 2016; Volume 4, pp. 199–217.
5. Hasson, S.; Lucarini, V.; Pascale, S. Hydrological cycle over South and Southeast Asian river basins as simulated by PCMDI/CMIP3 experiments. *Earth Syst. Dyn.* **2013**, *4*, 199–217.
6. Wake, C.P. Glaciochemical investigations as a tool for determining the spatial and seasonal variation of snow accumulation in the central Karakoram, northern Pakistan. *Ann. Glaciol.* **1989**, *13*, 279–284.
7. Annamalai, H.; Hamilton, K.; Sperber, K.R. The South Asian summer monsoon and its relationship with ENSO in the IPCC AR4 simulations. *J. Clim.* **2007**, *20*, 1071–1092.
8. Clift, P.D.; Plumb, R.A. *The Asian Monsoon: Causes, History and Effects*; Cambridge University Press: Cambridge, UK, 2008; Volume 270.
9. Bohner, J. General climatic controls and topoclimatic variations in Central and High Asia. *BOREAS* **2006**, *35*, 279–295.
10. Sperber, K.R.; Annamalai, H.; Kang, I.S.; Kitoh, A.; Moise, A.; Turner, A.; Wang, B.; Zhou, T. The Asian summer monsoon: An intercomparison of CMIP5 vs. CMIP3 simulations of the late 20th century. *Clim. Dyn.* **2013**, *41*, 2711–2744.
11. Wang, B.; Kang, I.S.; Lee, J.Y. Ensemble simulations of Asian-Australian monsoon variability by 11 AGCMs*. *J. Clim.* **2004**, *17*, 803–818.
12. Saha, A.; Ghosh, S.; Sahana, A.; Rao, E. Failure of CMIP5 climate models in simulating post-1950 decreasing trend of Indian monsoon. *Geophys. Res. Lett.* **2014**, *41*, 7323–7330.
13. Kang, I.S.; Jin, K.; Wang, B.; Lau, K.M.; Shukla, J.; Krishnamurthy, V.; Schubert, S.; Wailser, D.; Stern, W.; Kitoh, A.; et al. Intercomparison of the climatological variations of Asian summer monsoon precipitation simulated by 10 GCMs. *Clim. Dyn.* **2002**, *19*, 383–395.

14. Lin, J.L.; Weickman, K.M.; Kiladis, G.N.; Mapes, B.E.; Schubert, S.D.; Suarez, M.J.; Bacmeister, J.T.; Lee, M.I. Subseasonal variability associated with Asian summer monsoon simulated by 14 IPCC AR4 coupled GCMs. *J. Clim.* **2008**, *21*, 4541–4567.
15. Feng, X.; Porporato, A.; Rodriguez-Iturbe, I. Changes in rainfall seasonality in the tropics. *Nat. Clim. Chang.* **2013**, *3*, 811–815.
16. Pascale, S.; Lucarini, V.; Feng, X.; Porporato, A.; Hasson, S. Analysis of rainfall seasonality from observations and climate models. *Clim. Dyn.* **2015**, *44*, 3281–3301.
17. Favre, A.; Philippon, N.; Pohl, B.; Kalognomou, E.A.; Lennard, C.; Hewitson, B.; Nikulin, G.; Dosio, A.; Panitz, H.J.; Cerezo-Mota, R. Spatial distribution of precipitation annual cycles over South Africa in 10 CORDEX regional climate model present-day simulations. *Clim. Dyn.* **2016**, *46*, 1799–1818.
18. Chou, C.; Chiang, J.C.; Lan, C.W.; Chung, C.H.; Liao, Y.C.; Lee, C.J. Increase in the range between wet and dry season precipitation. *Nat. Geosci.* **2013**, *6*, 263–267.
19. Wang, B.; Lin, H. Rainy season of the asian-pacific summer monsoon. *J. Clim.* **2002**, *15*, 386–398.
20. Hasson, S.; Pascale, S.; Lucarini, V.; Böhner, J. Seasonal cycle of precipitation over major river basins in South and Southeast Asia: A review of the CMIP5 climate models data for present climate and future climate projections. *Atmos. Res.* **2016**, *180*, 42–63.
21. Geil, K.L.; Serra, Y.L.; Zeng, X. Assessment of CMIP5 model simulations of the North American monsoon system. *J. Clim.* **2013**, *26*, 8787–8801.
22. Hasson, S.; Lucarini, V.; Pascale, S.; Böhner, J. Seasonality of the hydrological cycle in major South and Southeast Asian river basins as simulated by PCMDI/CMIP3 experiments. *Earth Syst. Dyn.* **2014**, *5*, 67–87.
23. Sperber, K.R.; Annamalai, H. The use of fractional accumulated precipitation for the evaluation of the annual cycle of monsoons. *Clim. Dyn.* **2014**, *43*, 3219–3244.
24. Giorgi, F.; Jones, C.; Asrar, G.R. Addressing climate information needs at the regional level: The CORDEX framework. *World Meteorol. Org. (WMO) Bull.* **2009**, *58*, 175–183.
25. Jones, C.; Giorgi, F.; Asrar, G. The Coordinated Regional Downscaling Experiment: CORDEX, an international downscaling link to CMIP5. *CLIVAR Exch.* **2011**, *56*, 34–40.
26. Hao, Z.; Singh, V.P. Integrating entropy and copula theories for hydrologic modeling and analysis. *Entropy* **2015**, *17*, 2253–2280.
27. Pascale, S.; Lucarini, V.; Feng, X.; Porporato, A.; Hasson, S. Projected changes of rainfall seasonality and dry spells in a high greenhouse gas emissions scenario. *Clim. Dyn.* **2015**, *46*, 1331–1350.
28. Turner, A.G.; Annamalai, H. Climate change and the South Asian summer monsoon. *Nat. Clim. Chang.* **2012**, *2*, 587–595.
29. Bengtsson, L.; Hodges, K.I.; Roeckner, E. Storm tracks and climate change. *J. Clim.* **2006**, *19*, 3518–3543.
30. Fasullo, J.; Webster, P. A hydrological definition of Indian monsoon onset and withdrawal. *J. Clim.* **2003**, *16*, 3200–3211.
31. Li, C.; Yanai, M. The onset and interannual variability of the Asian summer monsoon in relation to land-sea thermal contrast. *J. Clim.* **1996**, *9*, 358–375.
32. Janowiak, J.E.; Xie, P. A global-scale examination of monsoon-related precipitation. *J. Clim.* **2003**, *16*, 4121–4133.
33. Krishnamurti, T.; Simon, A.; Thomas, A.; Mishra, A.; Sikka, D.; Niyogi, D.; Chakraborty, A.; Li, L. Modeling of forecast sensitivity on the march of monsoon isochrones from Kerala to New Delhi: The first 25 days. *J. Atmos. Sci.* **2012**, *69*, 2465–2487.
34. Hasson, S.; Lucarini, V.; Khan, M.; Petitta, M.; Bolch, T.; Gioli, G. Early 21st century snow cover state over the western river basins of the Indus River system. *Hydrol. Earth Syst. Sci.* **2014**, *18*, 4077–4100.
35. Yatagai, A.; Kamiguchi, K.; Arakawa, O.; Hamada, A.; Yasutomi, N.; Kitoh, A. APHRODITE: Constructing a long-term daily gridded precipitation dataset for Asia based on a dense network of rain gauges. *Bull. Am. Meteorol. Soc.* **2012**, *93*, 1401–1415.
36. Xie, P.; Janowiak, J.E.; Arkin, P.A.; Adler, R.; Gruber, A.; Ferraro, R.; Huffman, G.J.; Curtis, S. GPCP pentad precipitation analyses: An experimental dataset based on gauge observations and satellite estimates. *J. Clim.* **2003**, *16*, 2197–2214.
37. Xie, P.; Arkin, P.A. Global precipitation: A 17-year monthly analysis based on gauge observations, satellite estimates, and numerical model outputs. *Bull. Am. Meteorol. Soc.* **1997**, *78*, 2539.

38. Adler, R.F.; Huffman, G.J.; Chang, A.; Ferraro, R.; Xie, P.P.; Janowiak, J.; Rudolf, B.; Schneider, U.; Curtis, S.; Bolvin, D.; et al. The version-2 global precipitation climatology project (GPCP) monthly precipitation analysis (1979-present). *J. Hydrometeorol.* **2003**, *4*, 1147–1167.
39. Huffman, G.J.; Adler, R.F.; Bolvin, D.T.; Gu, G. Improving the global precipitation record: GPCP version 2.1. *Geophys. Res. Lett.* **2009**, *36*, doi:10.1029/2009GL040000.
40. Fekete, B.M.; Vörösmarty, C.J.; Roads, J.O.; Willmott, C.J. Uncertainties in precipitation and their impacts on runoff estimates. *J. Clim.* **2004**, *17*, 294–304.
41. Palazzi, E.; Hardenberg, J.; Provenzale, A. Precipitation in the Hindu-Kush Karakoram Himalaya: Observations and future scenarios. *J. Geophys. Res. Atmos.* **2013**, *118*, 85–100.
42. Prakash, S.; Mitra, A.K.; Momin, I.M.; Rajagopal, E.; Basu, S.; Collins, M.; Turner, A.G.; Achuta Rao, K.; Ashok, K. Seasonal intercomparison of observational rainfall datasets over India during the southwest monsoon season. *Int. J. Climatol.* **2015**, *35*, 2326–2338.
43. Taylor, K.E.; Stouffer, R.J.; Meehl, G.A. An overview of CMIP5 and the experiment design. *Bull. Am. Meteorol. Soc.* **2012**, *93*, 485–498.
44. McGregor, J.L.; Dix, M.R. An updated description of the conformal-cubic atmospheric model. In *High Resolution Numerical Modelling of the Atmosphere and Ocean*; Springer: New York, NY, USA, 2008; pp. 51–75.
45. Dix, M.; Vohralik, P.; Bi, D.; Rashid, H.; Marsland, S.; O'Farrell, S.; Uotila, P.; Hirst, A.; Kowalczyk, E.; Sullivan, A.; et al. The ACCESS coupled model: Documentation of core CMIP5 simulations and initial results. *Aust. Meteorol. Oceanogr. J.* **2013**, *63*, 83–99.
46. Gent, P.R.; Danabasoglu, G.; Donner, L.J.; Holland, M.M.; Hunke, E.C.; Jayne, S.R.; Lawrence, D.M.; Neale, R.B.; Rasch, P.J.; Vertenstein, M.; et al. The community climate system model version 4. *J. Clim.* **2011**, *24*, 4973–4991.
47. Voldoire, A.; Sanchez-Gomez, E.; y Mélia, D.S.; Decharme, B.; Cassou, C.; Sénési, S.; Valcke, S.; Beau, I.; Alias, A.; Chevallier, M.; et al. The CNRM-CM5. 1 global climate model: Description and basic evaluation. *Clim. Dyn.* **2013**, *40*, 2091–2121.
48. Samuelsson, P.; Jones, C.G.; Willén, U.; Ullerstig, A.; Gollvik, S.; Hansson, U.; Jansson, C.; Kjellström, E.; Nikulin, G.; Wyser, K. The Rossby Centre Regional Climate model RCA3: Model description and performance. *Tellus A* **2011**, *63*, 4–23.
49. Hazeleger, W.; Wang, X.; Severijns, C.; Ştefănescu, S.; Bintanja, R.; Sterl, A.; Wyser, K.; Semmler, T.; Yang, S.; Van den Hurk, B.; et al. EC-Earth V2. 2: Description and validation of a new seamless earth system prediction model. *Clim. Dyn.* **2012**, *39*, 2611–2629.
50. Griffies, S.M.; Winton, M.; Donner, L.J.; Horowitz, L.W.; Downes, S.M.; Farneti, R.; Gnanadesikan, A.; Hurlin, W.J.; Lee, H.C.; Liang, Z.; et al. The GFDL CM3 coupled climate model: Characteristics of the ocean and sea ice simulations. *J. Clim.* **2011**, *24*, 3520–3544.
51. Stevens, B.; Giorgetta, M.; Esch, M.; Mauritsen, T.; Crueger, T.; Rast, S.; Salzmann, M.; Schmidt, H.; Bader, J.; Block, K.; et al. Atmospheric component of the MPI-M Earth System Model: ECHAM6. *J. Adv. Model. Earth Syst.* **2013**, *5*, 146–172.
52. Sieck, K.; Raub, T.; Marien, L.; Buntemeyer, L.; Jacob, D. A new generation of the regional climate model REMO: REMO non-hydrostatic. In Proceedings of the EGU General Assembly Conference Abstracts, Vienna, Austria, 17–22 April 2016; Volume 18, p. 11945.
53. Saeed, F.; Hagemann, S.; Jacob, D. Impact of irrigation on the South Asian summer monsoon. *Geophys. Res. Lett.* **2009**, *36*, doi:10.1029/2009GL040625.
54. Thiessen, A.H. Precipitation averages for large areas. *Mon. Weather Rev.* **1911**, *39*, 1082–1089.
55. Mann, H.B. Nonparametric tests against trend. *Econom. J. Econom. Soc.* **1945**, *13*, 245–259.
56. Kendall, M. *Rank Correlation Methods*, 4th ed.; Charles Griffin: London, UK, 1975.
57. Theil, H. A rank-invariant method of linear and polynomial regression analysis. In *Collection of Henri Theil's Contributions to Economics and Econometrics*; Springer: Netherlands, 1992; pp. 345–381.
58. Sen, P.K. Estimates of the regression coefficient based on Kendall's tau. *J. Am. Stat. Assoc.* **1968**, *63*, 1379–1389.
59. Ghimire, S.; Choudhary, A.; Dimri, A. Assessment of the performance of CORDEX-South Asia experiments for monsoonal precipitation over the Himalayan region during present climate: Part I. *Clim. Dyn.* **2015**, 1–24, doi:10.1007/s00382-015-2747-2.

60. Syed, F.S.; Iqbal, W.; Syed, A.A.B.; Rasul, G. Uncertainties in the regional climate models simulations of South-Asian summer monsoon and climate change. *Clim. Dyn.* **2014**, *42*, 2079–2097.
61. Gao, X.; Shi, Y.; Zhang, D.; Wu, J.; Giorgi, F.; Ji, Z.; Wang, Y. Uncertainties in monsoon precipitation projections over China: Results from two high-resolution RCM simulations. *Clim. Res.* **2012**, *52*, 213–216.
62. Hasson, S.; Böhner, J.; Chishtie, F. Low Fidelity of Present-day Climate Modelling experiments and future climatic uncertainty over Himalayan watersheds of Indus basin. *Clim. Dyn.* **2016**, under review.
63. Mariotti, L.; Coppola, E.; Sylla, M.B.; Giorgi, F.; Piani, C. Regional climate model simulation of projected 21st century climate change over an all-Africa domain: Comparison analysis of nested and driving model results. *J. Geophys. Res. Atmos.* **2011**, *116*, doi:10.1029/2010JD015068.
64. Johnson, S.J.; Levine, R.C.; Turner, A.G.; Martin, G.M.; Woolnough, S.J.; Schiemann, R.; Mizielinski, M.S.; Roberts, M.J.; Vidale, P.L.; Demory, M.E.; et al. The resolution sensitivity of the South Asian monsoon and Indo-Pacific in a global 0.35 ° AGCM. *Clim. Dyn.* **2016**, *46*, 807–831.
65. Wehner, M.F.; Reed, K.A.; Li, F.; Bacmeister, J.; Chen, C.T.; Paciorek, C.; Gleckler, P.J.; Sperber, K.R.; Collins, W.D.; Gettelman, A.; et al. The effect of horizontal resolution on simulation quality in the Community Atmospheric Model, CAM5. 1. *J. Adv. Model. Earth Syst.* **2014**, *6*, 980–997.
66. Boos, W.R.; Hurley, J.V. Thermodynamic bias in the multimodel mean boreal summer monsoon. *J. Clim.* **2013**, *26*, 2279–2287.
67. Chakraborty, A.; Nanjundiah, R.; Srinivasan, J. Role of Asian and African orography in Indian summer monsoon. *Geophys. Res. Lett.* **2002**, *29*, 50–51.
68. Chakraborty, A.; Nanjundiah, R.; Srinivasan, J. Theoretical aspects of the onset of Indian summer monsoon from perturbed orography simulations in a GCM. *Ann. Geophys.* **2006**, *24*, 2075–2089.
69. Saeed, F.; Hagemann, S.; Saeed, S.; Jacob, D. Influence of mid-latitude circulation on upper Indus basin precipitation: The explicit role of irrigation. *Clim. Dyn.* **2013**, *40*, 21–38.
70. Levine, R.C.; Turner, A.G. Dependence of Indian monsoon rainfall on moisture fluxes across the Arabian Sea and the impact of coupled model sea surface temperature biases. *Clim. Dyn.* **2012**, *38*, 2167–2190.
71. Levine, R.C.; Turner, A.G.; Marathayil, D.; Martin, G.M. The role of northern Arabian Sea surface temperature biases in CMIP5 model simulations and future projections of Indian summer monsoon rainfall. *Clim. Dyn.* **2013**, *41*, 155–172.
72. Sandeep, S.; Ajayamohan, R. Poleward shift in Indian summer monsoon low level jetstream under global warming. *Clim. Dyn.* **2015**, *45*, 337–351.
73. Sandeep, S.; Ajayamohan, R. Origin of cold bias over the Arabian Sea in climate models. *Sci. Rep.* **2014**, *4*, doi:10.1038/srep06403.
74. Laprise, R.; Hernández-Díaz, L.; Tete, K.; Sushama, L.; Šeparović, L.; Martynov, A.; Winger, K.; Valin, M. Climate projections over CORDEX Africa domain using the fifth-generation Canadian Regional Climate Model (CRCM5). *Clim. Dyn.* **2013**, *41*, 3219–3246.
75. Dosio, A.; Panitz, H.J.; Schubert-Frisius, M.; Lüthi, D. Dynamical downscaling of CMIP5 global circulation models over CORDEX-Africa with COSMO-CLM: Evaluation over the present climate and analysis of the added value. *Clim. Dyn.* **2015**, *44*, 2637–2661.
76. Islam, S.; Rehman, N.; Sheikh, M.; Khan, A. *Climate Change Projections for Pakistan, Nepal and Bangladesh for SRES A2 and A1B Scenarios Using Outputs of 17 GCMs Used in IPCC-AR4*; Technical Report, GCISC-RR-03; Global Change Impact Studies Centre (GCISC): Islamabad, Pakistan, 2009.
77. Syed, F.S.; Islam, S.; Rehman, N.; Sheikh, M.M.; Khan, A.M. *Climate Change Scenarios for Pakistan and Some South Asian Countries for SRES A2 and B2 Scenarios Based on Six Different GCMs Used in IPCC-TAR*; Technical Report GCISC-RR-02; Global Change Impact Studies Centre (GCISC): Islamabad, Pakistan, 2009.
78. Islam, S.; Rehman, N.; Sheikh, M.M.; Khan, A.M. *High Resolution Climate Change Scenarios Over South Asia Region Donscaled by Regional Climate Model PRECIS for IPCC SRES A2 Scneario*; Technical Report GCISC-RR-06; Global Change Impact Studies Centre (GCISC): Islamabad, Pakistan, 2009.
79. Kulkarni, A.; Patwardhan, S.; Kumar, K.K.; Ashok, K.; Krishnan, R. Projected climate change in the Hindu Kush-Himalayan region by using the high-resolution regional climate model PRECIS. *Mt. Res. Dev.* **2013**, *33*, 142–151.
80. Rajbhandari, R.; Shrestha, A.; Kulkarni, A.; Patwardhan, S.; Bajracharya, S. Projected changes in climate over the Indus river basin using a high resolution regional climate model (PRECIS). *Clim. Dyn.* **2015**, *44*, 339–357.

81. Iqbal, W.; Syed, F.; Sajjad, H.; Nikulin, G.; Kjellström, E.; Hannachi, A. Mean climate and representation of jet streams in the CORDEX South Asia simulations by the regional climate model RCA4. *Theor. Appl. Climatol.* **2016**, 1–19, doi:10.1007/s00704-016-1755-4.
82. Dimri, A.P. Wintertime land surface characteristics in climatic simulations over the western Himalayas. *J. Earth Syst. Sci.* **2012**, *121*, 329–344.
83. Sabeerali, C.; Rao, S.A.; Dhakate, A.; Salunke, K.; Goswami, B. Why ensemble mean projection of south Asian monsoon rainfall by CMIP5 models is not reliable? *Clim. Dyn.* **2015**, *45*, 161–174.
84. Mishra, V. Climatic uncertainty in Himalayan water towers. *J. Geophys. Res. Atmos.* **2015**, *120*, 2689–2705.
85. Ramanathan, V.; Chung, C.; Kim, D.; Bettge, T.; Buja, L.; Kiehl, J.; Washington, W.; Fu, Q.; Sikka, D.; Wild, M. Atmospheric brown clouds: Impacts on South Asian climate and hydrological cycle. *Proc. Natl. Acad. Sci. USA* **2005**, *102*, 5326–5333.
86. Ramesh, K.; Goswami, P. Assessing reliability of regional climate projections: The case of Indian monsoon. *Sci. Rep.* **2014**, *4*, 4071.
87. Hasson, S.; Böhner, J.; Lucarini, V. Prevailing climatic trends and runoff response from Hindukush–Karakoram–Himalaya, upper Indus basin. *Earth Syst. Dyn. Discus.* **2015**, *6*, 579–653.